Designer Based Fourier Transformed Voltammetry: A Multi-frequency, Variable Amplitude, Sinusoidal Waveform

Yongjun Tan[a, 1] Gareth P. Stevenson[b] Ruth E. Baker[c]
Darrell Elton[d] Kathryn Gillow[b] Jie Zhang[e]
Alan M. Bond[a, *] David J. Gavaghan[b, *]

[a]School of Chemistry, Monash University, Clayton, Melbourne, Victoria 3800, Australia.

[b]Oxford University Computing Laboratory, Wolfson Building, Parks Road, Oxford, OX1 3QD, United Kingdom.

[c]Centre for Mathematical Biology, Mathematical Institute, 24-29 St. Giles', Oxford OX1 3LB, United Kingdom.

[d]Department of Electronic Engineering, Latrobe University, Bundoora, Victoria 3083, Australia.

[e]Institute of Bioengineering and Nanotechnology, 31 Biopolis Way, The Nanos, Singapore 138669.

[1]Present address: School of Applied Chemistry, Curtin University of Technology, Perth, Australia.

[*]Corresponding authors. Alan M. Bond, email: Alan.Bond@sci.monash.edu.au, telephone: +61 3 9905 1338, fax: +61 3 9905 4597. David J. Gavaghan, email: David.Gavaghan@comlab.ox.ac.uk, telephone: +44 1865 610667, fax: +44 1865 610670.

Abstract

Fourier transform methods allow custom-designed complex waveforms to be used in ac voltammetry. Commonly a single wave or sum of sine waves of variable angular frequency (ω) but constant amplitude (ΔE) superimposed onto a dc ramp are employed. In the present case, a custom-designed waveform consisting of a combination of eight sine waves is introduced, with the property that each sine wave within the composite waveform has the property $\Delta E_i \propto 1/\sqrt{\omega_i}$ where i represents the i^{th} sine wave. Frequencies (and amplitudes) employed in a single experiment cover the range from 34.94 Hz (20 mV) to 1970.01 Hz (2.66 mV). Reversibility is readily detected via use of this designer waveform by noting a constant peak height ($I_p(\omega t)$) for all eight frequencies, whereas $I_p(\omega t)$ values decrease in a characteristic manner with increasing frequency or when uncompensated resistance is present, as demonstrated experimentally and theoretically. Importantly, background charging current contributions do not increase to a level that makes measurement of faradaic current difficult at high frequencies and hence charging current is readily corrected for over the entire frequency range of interest.

Keywords: designer ac waveform, Fourier transform voltammetry, variable amplitude and frequency.

1 Introduction

During the last decade, quantitative use of the technique of Fourier transformed (FT) ac voltammetry has been expanded [1, 2] to accommodate large levels of nonlinearity introduced by application of potential perturbations with amplitudes much larger than those customarily employed in ac voltammetry or impedance spectroscopy [3]. Typically, in these recent studies, a sinusoidal waveform of amplitude up to 200 mV with a frequency of 10 Hz–50 kHz is superimposed onto the triangular waveform used in dc cyclic voltammetry. The large amplitude method, when analysed in the frequency domain via a Fourier transform-inverse Fourier transform sequence, provides simultaneous access to the dc and fundamental harmonic ac responses, in addition to higher ac harmonics that emerge from the nonlinearity. This large-amplitude FT ac technique is advantageous in studies of electrode kinetics because of the well-defined patterns of behaviour that emerge in the now readily detected higher harmonics [4], with minimal problem from charging current. The large amplitude technique has been applied successfully to elucidate details of the electrochemistry of complex electrode processes such as surface-bound azurin [5] and mediated oxidation of acerbic acid by ferrocenemethanol [6].

Theoretical treatments for the sinusoidal version of the large-amplitude FT-ac method have been developed by Engblom and Oldham et al. [1] and Gavaghan and Bond et al. [2, 7–9]. Furthermore, recent work from several laboratories has demonstrated that instrumentation can be developed in which a periodic ac waveform of any amplitude may be superimposed onto a linear or triangular dc voltage [1, 2, 5, 8, 10]. Gavaghan et al. have also described a large amplitude FT square wave ac method that has been termed 'square-wave voltammetry in the frequency domain' [9]. Other waveforms have also been suggested that are based on the Fourier series of sawtooth or other waveforms. Custom-designed instrumentation has been developed to specifically accommodate the sinusoidal and the other variations of the FT-ac technique [11, 12].

As part of our effort to further develop the FT-ac voltammetric technique, we now introduce a multi-frequency and variable amplitude waveform. The

concept behind this initial development of a designer waveform for characterising a particular class of electrochemical processes is to identify combinations of sine waves that allow the rapid identification of the nature of charge transfer processes described by Equation (1) where $E^{o'}$ is the reversible formal potential, $k^{o'}$ is the heterogeneous charge transfer rate constant at $E^{o'}$, n is the number of electrons transferred and α is the charge transfer coefficient.

$$A + ne^- \underset{}{\overset{\alpha,\, k^{o'},\, E^{o'}}{\rightleftharpoons}} B \tag{1}$$

The waveform introduced for identifying reversibility in this paper is a combination of sine waves, with the property that each sine wave within the composite waveform has the property $\Delta E_i \propto 1/\sqrt{\omega_i}$, where ω_i and ΔE_i are the angular frequency and the amplitude of the i^{th} sine wave respectively. The concept is based on the analytical solution available in small amplitude ac voltammetry when a single sine wave is applied, under conditions of planar diffusion,

$$I(\omega t) = \frac{n^2F^2Ac_A(\omega D_A)^{\frac{1}{2}}\Delta E}{4RT\cosh^2\left(\frac{j}{2}\right)}\sin\left(\omega t + \frac{\pi}{4}\right), \tag{2}$$

where A is the electrode area, c_A is the concentration of species A, n is the number of electrons transferred ($n = 1$ in the present case), D_A is the diffusion coefficient of species A, t is time, $j = nF(E_{\text{dc}} - E^{o'})/RT$ and E_{dc} is the dc component of the applied potential, $E_{\text{dc}} = E_{\text{initial}} + vt$, where E_{initial} is the starting potential and v is the scan rate.

Thus, under conditions where this relationship holds, and a waveform where $\Delta E_i \propto 1/\sqrt{\omega_i}$ is applied in a single experiment the fundamental harmonic peak current is such that $I_p(\omega t) \propto \omega^{\frac{1}{2}}\Delta E$. Reversibility, achieved when $k^{o'}$ is very large, is rapidly recognised when using the custom-designed waveform by detection of a fundamental harmonic peak height ($I_p(\omega t)$) that is independent of frequency. In the case of quasi-reversibility, a characteristic frequency dependence is also detected in which $I_p(\omega t)$ decreases with increasing frequency, as also occurs if uncompensated resistance is significant. Finally, it is noted that traditionally when waveforms with constant ΔE values are used, the background current, which is proportional to ω, becomes very large at high frequencies, making the faradaic current hard to detect. In the present case, the background current does not increase very dramatically with frequency and hence correction,

even at high frequencies, is facilitated.

2 Experimental

2.1 Instrumentation

Details of the FT-ac voltammetric instrumentation are provided in [13]. Initial estimates of the uncompensated resistance (R_u) values were obtained using a BAS (Bioanalytical Systems)-Epsilon potentiostat and applying a small potential step in a potential region where no faradaic current flows. Analysis of the charging current versus time curve allows R_u to be extracted, as described in reference [6].

2.1.1 Chemicals and reagents

All chemicals and the solvent dichloromethane were of reagent grade purity and used as received from the manufacturer (Aldrich). The deionized water was obtained from a MilliQ-MilliRho purification system.

2.1.2 Instrumentation and procedures

A conventional single compartment, three-electrode cell was employed in all voltammetric measurements, with glassy-carbon (GC, 7.07 mm^2), platinum (Pt, 3.14 mm^2) or gold (Au, 3.14 mm^2) macrodisk working electrodes, an Ag | AgCl (0.5 M KCl) reference electrode and a platinum wire auxiliary electrode. The disc-shaped working electrodes were constructed by sealing glassy-carbon or metal rods into insulating Kel-F sheaths with epoxy resin. Before use, the surfaces of these electrodes were manually polished with an aqueous slurry of 0.1 or 0.05 μm alumina particles (Bioanalytical Systems) on a Microcloth polishing cloth (Buehler, Lake Bluff, IL) and then rinsed thoroughly with water.

In initial experiments, GC, Au or Pt electrodes were immersed in 10 ml of aqueous solutions containing 0.100 mM; 0.202 mM; 0.300 mM; 0.404 mM; 1.00 mM or 2.00 mM Ferrocenemethanol (FcMeOH) with 0.50 M KCl as the supporting electrolyte. The oxidation of FcMeOH was used as an example of a reversible process. Other systems studied were: reduction of $[Ru(NH_3)_6]^{3+}$ (reversible)

and $[Fe(CN)_6]^{3-}$ (quasi-reversible), again in 0.50 M KCl aqueous electrolyte; and oxidation of FcMeOH (reversible) in dichloromethane (0.1 M Bu_4NPF_6). The latter was used to assess the impact of a high level of uncompensated resistance. Solutions were purged with nitrogen for at least 5 minutes prior to commencement of a voltammetric experiment. All experiments were carried out at (20±1)°C.

The waveform used in the FT-ac voltammetric experiments was a composite, eight component sine-wave signal superimposed onto the dc potential to give a total potential E_t where

$$E_t = E_{\mathrm{dc}} + \sum_{i=1}^{8} \Delta E_i \sin(\omega_i t), \tag{3}$$

with the frequencies, ω_i, and amplitudes, ΔE_i, as given in Table 1. The individual sine waves were not phase randomised, as is sometimes the case in experiments where all amplitudes are the same [11]. However, consideration was given to minimisation of overlap of higher harmonic terms on the basis of an algorithm available in the literature [11]. Instrumental and FT requirements mean that 2^n data points need to be obtained. The chosen scan rate and potential range specified in Table 1 meant that the combination given there was identified as being suitable for implementation of the designer waveform with minimal overlap from higher harmonic and frequency sum and difference terms. In particular, these nonlinear terms were not within 5–10 Hz of the 8 applied frequencies. The amplitudes were chosen to be in the range of 20 to 2 mV and the frequencies ranging from 34.94 to 1970.01 Hz are geometrically spaced over a range that allows a substantial faradaic component to be measured relative to background current, under all conditions. However, it may be noted that the number of sine waves chosen in the designer waveform need not be 8, nor have the specific frequencies selected for the present study.

2.1.3 Data analysis and simulations

The experimental data, obtained with the FT-ac instrumentation, yield current, time, and applied dc potential as the output information. The data are plotted as current versus time and then transformed into frequency-related power

spectra for further analysis.

The raw FT-ac data obtained from experiments contains a very large number of data points (2^{18}). Consequently, processing the full set of data is slow. For this reason, a 'decimation' data reduction process is implemented in the frequency domain, where the first 2^{15} data points present in the raw data are retained and all the higher frequency data is discarded before the inverse Fourier transform operation is applied. This strategy removes data that contains no information relevant to the electrochemical reaction ($> 2,000$ Hz) being studied, and significantly reduces the data file size needed for the iFT operation while maintaining all useful information.

Another problem with raw ac data is the presence of background (charging) current. It is well known that in the fundamental harmonic response, the background current may dominate the voltammetry, particularly at high frequency, so that quantitative analysis of the faradaic component associated with electron transfer may require employment of a background correction procedure. Measurement of the background current at selected potential ranges on both sides of the region where Faradaic current is detected, interpolation to give values in this potential region using a polynomial fit and vectorial subtraction of the calculated background were used in the present case. The background current does not contribute significantly to the second and higher harmonic ac voltammograms. Consequently, background correction is unnecessary for measurement of these higher order components.

Analysis of the kinetics was based on peak height versus frequency profiles. However, full simulations were carried out using the procedure described below. Fitting of experimental data with simulated results for the quasi-reversible process was undertaken in an essentially heuristic manner:

Step 1. Identify the reversibility or otherwise of an electrode process by examining the lowest concentration data set, where the IR_u influence should be minimal, and compare it against predictions based on the reversible case (i.e. $I_p(\omega t)$ is constant for all 8 sine waves). If $I_p(\omega t)$ is independent of frequency, then the system under study is concluded to be reversible.

Step 2. Analyse data at higher concentrations and check if $I_p(\omega t)$ versus fre-

quency profiles are independent of concentration. If concentration dependence is detected, check if it is consistent with the increasing importance of the IR_u drop.

Step 3. To determine the contribution from the IR_u drop or quasi-reversibility, make initial estimates of values for parameters needed in numerical simulation. For instance, make an initial estimate of the value of $E^{o'}$, using $E^{o'} = (E_p^{\text{ox}} + E_p^{\text{red}})/2$, where E_p^{ox} and E_p^{red} are the peak potentials for the oxidation and reduction currents, respectively, in the aperiodic dc component. R_u can be evaluated immediately, as described in reference [6], and C_{dl} can be estimated from the magnitude of the fundamental harmonic current. In this study, initial guesses of diffusion coefficient values (D) are taken from the literature [6, 14–16] and are 7.6×10^{-6} cm^2 s^{-1} for FcMeOH, 8.0×10^{-6} cm^2 s^{-1} for $[Ru(NH_3)_6]^{3+}$ and 6.3×10^{-6} cm^2 s^{-1} for $[Fe(CN)_4]^{3-}$. In practice it was found that a value of $7.6 \pm 0.5 \times 10^{-6}$ cm^2 s^{-1} could be used for all three species in 0.50 M KCl under conditions of the present study.

Step 4. Compare simulations against experimental results until the level of desired accuracy is reached. Estimates of $E^{o'}$, D and R_u (k_0 and α if required) may need to be refined by comparing simulated and experimental peak currents, and wave shapes.

2.2 Simulations

We consider only the case of a macro-disk electrode: in doing so, we follow previous work [2, 8, 9] and invoke the assumption that diffusion is a one dimensional process.

2.2.1 Modelling the reaction mechanism

The system considered is one of semi-infinite mass transport to a planar electrode where a simple reduction or oxidation reaction occurs. This type of reac-

tion is commonly referred to as an E process and is represented as follows,

$$A + ne^- \underset{k_b}{\overset{k_f}{\rightleftharpoons}} B, \tag{4}$$

where both A and B are soluble in the solution phase; k_f and k_b are the forward and backward potential-dependent rate constants associated with Butler-Volmer kinetics [17], given by

$$k_f = k_0^{'} \exp\left(-\frac{\alpha n F}{RT}[E(t) - E^{o'} - I(t)R_u]\right), \tag{5}$$

$$k_b = k_0^{'} \exp\left((1-\alpha)\frac{nF}{RT}[E(t) - E^{o'} - I(t)R_u]\right), \tag{6}$$

with $E(t)$ being the applied potential (the exact form of which is described in the next paragraph), R_u is the uncompensated resistance, $I(t)$ is the total current and all other symbols as defined previously or as conventionally used.

The number of electrons transferred in the reaction, n, may be assigned as positive or negative so that both oxidation and reduction reactions are covered by the treatment that follows. By convention, our voltammetric experiments will begin at time $t = 0$: at time $t < 0$ the electrode is held at a constant initial potential, E_i, which is sufficiently extreme to ensure that the reaction in Equation (4) does not occur significantly. For $t > 0$, the time-dependent applied potential $E(t)$ has two components, a dc ramp denoted by $E_{\rm dc}$, and an oscillatory component which constitutes the 'designer' waveform represented by $E_{\rm ac} = \sum_{i=1}^{8} \Delta E_i \sin(\omega_i t)$, where ΔE_i are the amplitudes corresponding to each of the frequencies, ω_i, respectively, and these obey the following relation $\Delta E_i = \Delta E_1/\sqrt{\omega_i/\omega_1}$, where ΔE_1 is the amplitude of the first sine wave and ω_1 is the corresponding frequency. Note that we are using eight sine waves to mimic what has been done in the experiments. However, the theory can be applied to as many sine waves as may be desired by the user. Therefore the potential is given by the relationship

$$E(t) = E_{\rm dc}(t) + E_{\rm ac}(t), \tag{7}$$

$$= E_{\rm i} + vt + \sum_{i=1}^{8} \Delta E_i \sin(\omega_i t), \tag{8}$$

where v is the scan rate and has the same sign as n and $E_{\rm i}$ is the initial dc

potential. Also we have that

$$I(t) = I_f(t) + I_c(t), \tag{9}$$

$$\text{where} \quad I_c = C_{\text{dl}} \frac{\mathrm{d}E}{\mathrm{d}t}, \tag{10}$$

I_c is referred to as the capacitive current and I_f is the faradaic current (see definition in Section 2.2.2).

Mass transport to the electrode is then modelled by a linear diffusion equation for each species (A, B). If we let $c_{\text{A}}(x,t)$ and $c_{\text{B}}(x,t)$ represent the concentrations of species A and B, respectively, and let x represent the distance from the electrode surface at time t, we get the following system of equations,

$$\frac{\partial c_{\text{A}}}{\partial t} = D_{\text{A}} \frac{\partial^2 c_{\text{A}}}{\partial x^2}, \tag{11}$$

$$\frac{\partial c_{\text{B}}}{\partial t} = D_{\text{B}} \frac{\partial^2 c_{\text{B}}}{\partial x^2}, \tag{12}$$

where D_{A} and D_{B} are the diffusion coefficients for each of the species A and B, respectively.

In many studies, microelectrodes (radial diffusion dominant) are used instead of macroelectrodes (linear diffusion dominant) in order to minimise the IR_u drop and the charging current. We have previously studied the effects of the use of microelectrodes in ac voltammetry [7] and have derived precise conditions under which the effects of radial diffusion can be neglected. This work demonstrates, both theoretically and experimentally, that the effects of radial diffusion are much lower in the ac voltammetry case and these results carry through directly tot he designer waveform introduced in this paper.

2.2.2 Boundary conditions

Given that we have made the assumption of semi-infinite linear diffusion, we have the following boundary and initial conditions:

$$\text{at } x = 0 \quad D_{\text{A}} \frac{\partial c_{\text{A}}}{\partial x} = -D_{\text{B}} \frac{\partial c_{\text{B}}}{\partial x} = \frac{I_f(t)}{nAF} = k_f c_A - k_b c_B; \tag{13}$$

$$\text{as } x \to \infty \quad c_{\text{A}} = c_{\text{A}}^*, \quad c_{\text{B}} = 0; \tag{14}$$

$$\text{and at } t = 0 \quad c_{\text{A}} = c_{\text{A}}^*, \quad c_{\text{B}} = 0. \tag{15}$$

Here, c_{A}^{*} is the bulk concentration of species A and $I_f(t)$ is the faradaic current. Note that the equation involving $I_f(t)$ in Equation (13) is derived from Fick's first and Faraday's laws.

2.2.3 Non-dimensional variables

As has been discussed elsewhere [8, 18], we re-cast the problem in terms of non-dimensional variables: these dimensionless variables will be assigned Greek symbols in order to improve clarity. The nature of the problem implies a linear relationship between time t and the dc component of applied potential, E_{dc}, therefore the dimensionless symbol τ can be defined by

$$\tau = F(E_{\mathrm{init}} + vt - E^{o'})/RT = F(E_{\mathrm{dc}} - E^{o'})/RT, \tag{16}$$

and is used to replace both of these dimensional variables.

The sine wave amplitudes ΔE_i are similarly non-dimensionalised to obtain

$$\Delta\tau_i = \frac{F\Delta E_i}{RT}, \tag{17}$$

whilst the angular frequency ω_i becomes

$$\Omega_i = \frac{RT\omega_i}{Fv}. \tag{18}$$

This now allows us to write down a non-dimensional version of Equation (8), using Equations (16)-(18), where $\epsilon(\tau)$ is the non-dimensional potential

$$\epsilon(\tau) = \epsilon_{\mathrm{dc}}(\tau) + \epsilon_{\mathrm{ac}}(t), \tag{19}$$

$$= \tau + \sum_{i=1}^{8} \Delta\tau_i \sin(\Omega_i \tau). \tag{20}$$

Note that R_u and $I_{\mathrm{tot}}(t)$ are nondimensionalised as follows

$$\rho_u = \frac{F^2 A D_A c_A^*}{RT}\left(\frac{vF}{D_A RT}\right)^{\frac{1}{2}} R_u, \tag{21}$$

$$\iota_{\mathrm{tot}}(\tau) = \left(\frac{D_A RT}{vF}\right)^{\frac{1}{2}} \frac{I_{\mathrm{tot}}(t)}{AFD_A c_A^*}; \tag{22}$$

faradaic and capacitive currents are non-dimensionalised in the same way as for the total current, $I_{\mathrm{tot}}(t)$. Finally the double layer capacitance constant is non-dimensionalised as follows

$$\gamma_{\mathrm{dl}} = \left(\frac{D_A RT}{Fv}\right)^{\frac{1}{2}} \frac{vC_{\mathrm{dl}}}{AFD_A c_A^*}. \tag{23}$$

2.2.4 Numerical methods

The numerical algorithm used to solve the equations in Section 2.2.1 involves backward Euler discretisations [19], along with a simple expanding mesh in space, as described in [2]. We also make use of Brent's method to deal with the nonlinearity introduced via the inclusion of uncompensated resistance and double layer capacitance [20].

Data analysis of simulation results is carried out in the frequency domain using Fourier analysis (via FFTs). This allows us to pick out the dc component of the signal as well as the harmonics of interest in a straightforward manner, again as described previously in [2]. The 'decimation' process is done in the frequency domain, where the first 2^n data points are retained and the data at higher frequencies is discarded before the inverse Fourier transform is applied.

3 Results and discussion

3.1 Experimental aspects of multi-frequency and variable amplitude ac voltammetry for a reversible process

Figure 1 illustrates the steps required for analysis of an electrode process after collection of data in the *I-t* format, using the multi-frequency and variable-amplitude designer waveform FT-ac voltammetry. The example presented is for the oxidation of moderately low 0.404 mM concentration of FcMeOH in aqueous 0.5 M KCl electrolyte at a GC electrode. According to literature reports [6]. FcMeOH is oxidised reversibly to $[\text{FcMeOH}]^+$ by a simple, outer-sphere, one-electron charge transfer process

$$\text{FcMeOH} \rightleftharpoons [\text{FcMeOH}]^+ + e^-. \tag{24}$$

Figure 1(a) demonstrates clearly that this new designer form of FT-ac voltammetry generates a vast amount of data which can be displayed in the *I-t* format (Figures 1(a) and (b))), or as the power spectrum (Figure 1(c)) in the frequency domain. The power spectrum provides a convenient overview of the relative significance of dc and ac terms. The 'noisy' nature of the power spectrum (Figure 1(c)) implies, as expected, that this new form of ac voltammetry contains a very large amount of ac harmonic information. The dc aperiodic component (Figure 1(d)), the fundamental (Figure 1(e)–(g)), higher ac harmonics (Figure 1(h)–(n)) and frequency sum and difference terms (not shown), are derived by use of the power spectrum and the inverse FT algorithm. For the medium to fairly small amplitude case used in experimental studies, the second ac harmonic component (Figure 1(j)) may be identified at all frequencies, although the third harmonic (Figure 1(m)) can become obscured by the system noise. In the highest frequency, minimum ΔE, case, where $\Delta E = 2.66$ mV, the contribution from nonlinearity is minimal.

In order to display the harmonic information in a clearer form, the eight fundamental harmonics can be presented in raw (Figures 2(a) and (b)), decimated (Figures 2(c) and (d)) and background corrected (Figures 2(e) and (f)) format,

which readily reveals the peak current $I_p(\omega t)$, values associated with each of the eight frequencies in the designer waveform.

Figure 2(d) depicts the fundamental harmonic response for the 8 frequencies in ac *I-t* format after applying the 'decimation' process. The result is indistinguishable from that produced by analysis of the full data set (Figure 2(b)).

A significant frequency-dependent background charging current contribution is clearly observable in the fundamental ac harmonics (Figure 2(b)). The background current corrected results in Figure 2(f) reveal that the peak heights associated with the Faradaic process are independent of frequency, within experimental error, as predicted theoretically for a reversible process.

3.2 Simulation of the FT-ac voltammetry

Simulations of the fundamental harmonic ac voltammetry obtained for a reversible process ($k_0^{'} = 10,000$ cm s^{-1} and $\alpha = 0.5$) with the designer waveform and parameters given in Table 1 along with: $R_u = 0$ Ω; $C_{\rm dl} = 0.09$ Fm^{-2}; $E^{o'} = 0.185$ V; and $D = 7.6 \times 10^{-6}$ cm^2 s^{-1} (Figure S-1(a) and (b)), are in excellent agreement with experimental data (provided in Figure 2(a) and (b)).

If zero capacitance is employed instead of 0.09 F m^{-2} in the simulation, as is the case in Figure S-2, then excellent agreement is achieved with background current corrected experimental data given in Figure 2(e) and (f). This result demonstrates the effectiveness of background current correction software used in this study.

3.3 Application of the designer waveform to the [FcMeOH]$^{0/+}$ process as a function of concentration

Ideally, the reversible [FcMeOH]$^{0/+}$ process should exhibit $I_p(\omega t)$ values that are independent of frequency for all concentrations, when using the designer waveform. This is true for FcMeOH concentrations ≤ 0.404 mM (see Figure S-2 for 0.404 mM case). However, less conformity to this predicted response was obtained at higher FcMeOH concentrations. In particular, significant de-

viation from $I_p(\omega t)$ being independent of frequency was obtained (Figure 3) with a 2.00 mM FcMeOH solution, even though the background correction is relatively unimportant for this data set. Data obtained at $\geq$ 1 mM FCMeOH concentration resemble that expected for a quasi-reversible process.

The major factor contributing to the apparently non-reversible behaviour at higher FcMeOH concentrations is the presence of an uncompensated (Ohmic) IR_u drop which becomes more important as the concentration (current) is increased. The IR_u drop can lead to significant distortion in FT-ac voltammetry [13]. The predicted effect on designer-waveform FT-ac voltammetry is illustrated by simulations shown in Figure 4, with $R_u = 100\ \Omega$. In the present experiment at a GC electrode with 0.50 M KCl as the electrolyte, R_u is experimentally estimated to be 20 Ω. Simulations confirm that this value is not expected to be important at low concentrations of FcMeOH but, as found experimentally, does have an impact upon data of concentrations $\geq$ 1 mM.

For the theory of the designer waveform to be fully valid, surface interactions between FcMeOH (or $[FcMeOH]^+$) and the electrode should be absent. A useful method of checking for surface interaction is to compare the background current in 0.50 M KCl before and after addition of FcMeOH. As shown in Figure S-3, the background current at the glassy carbon electrode is reduced by a small amount after addition of 2.0 mM FcMeOH to 0.50 M KCl electrolyte. No differences in background current were detected on addition of FcMeOH concentrations $\leq$ 0.404 mM. The implication of this result is that FcMeOH (and $[FcMeOH]^+$) adsorbs weakly onto a glassy carbon electrode, resulting in a small reduction in the double layer capacitance. In contrast the background current at platinum and gold electrodes in 0.50 M KCl is indistinguishable in the presence or absence of 2.0 mM FcMeOH, which indicates that FcMeOH does not adsorb at a detectable level at these electrode surfaces. Additionally, R_u is only 10 Ω at these electrode surfaces compared to 20 Ω at the GC electrode so that $I_p(\omega t)$ values at platinum or gold electrodes, even with 2.0 mM FcMeOH present, are closer to a constant than at the GC surface. Clearly, taking R_u and surface interactions into account may be necessary if the use of the designer-waveform to detect reversibility is to be correctly implemented.

Clearly, background current correction becomes highly critical, particularly at high frequencies and low concentrations of FcMeOH, where the background current may produce a significant component of the total current. Figure S-4 illustrates the FT-ac voltammetry at a GC electrode in 0.50 M KCl electrolyte with 0.100 mM FcMeOH.

The instrumental background current correction implemented in this work uses baseline-subtraction software in a user-interactive mode. Thus, data are chosen at user-selected times at either side of the $[FcMeOH]^{0/+}$ or other process. A polynomial fit to both data sets and interpolation to potentials in between, leads to a predicted background at potentials where a Faradaic current is present. Obviously, there is a small level of uncertainty in this approach. Figure S-4 contains the background corrected faradaic current, for a dilute 0.100 mM FcMeOH solution using the polynomial fit derived from either 0.5–1.5 and 11–12 s, or 0–1 and 10–11 s zones for the correction of the raw data. Even with this more severe background problem than used in studies at higher concentration referred to above, excellent correction is still achieved. Traditionally, all sine waves used in multi-waveform approaches use constant values of ΔE and so the background current increases with frequency. The designer-waveform mitigates problems with large background current at higher frequencies.

An alternative means of background current correction is to undertake measurements in the base electrolyte to produce the 'blank background current file'. When 0.50 M KCl was used to produce the 'blank background current file' for correction of experimental data, this form of correction worked well at gold and platinum electrodes. However, it should be noted that this 'blank background current file' correction method is applicable only if adsorption is negligible, which is not perfectly true when high concentrations of FcMeOH are oxidised at a GC electrode. In general, the instrumental method is rapid and reliable, provided the zones used for background fitting are selected sensibly. This method is therefore recommended as a generally applicable and convenient approach for dealing with the background current correction.

3.4 Comparison of the designer waveform with other FT–ac methods

An alternative approach to the use of the designer waveform introduced in this study is to use eight sine waves individually in eight experiments instead of simultaneously in just one experiment. $I_p(\omega t)$ values using this single sine wave version are similar (Figure 5). However, the ability to obtain all data from a single experiment is clearly a significant advantage of the far more efficient designer waveform. Alternatively, one can employ the same frequency set as in Table 1 but with a constant amplitude for all frequencies. Data obtained from this more conventional experiment with $\Delta E = 15$ mV for all frequencies are shown in Figure 6. As expected, the values of $I_p(\omega t)$ now increase with frequency. However, the IR_u drop now becomes even more significant at higher frequencies, as does the background current.

Another alternative is to use a square-wave FT-ac method [9, 21–23] which utilises a variable amplitude waveform at frequencies ωt, $3\omega t$, $5\omega t$ etc. A square-wave experiment is equivalent to applying $k = (K + 1)/2$ sine waves of varying amplitude where K is an odd natural number [23]. In this case, the square-wave can be written as

$$E_{\text{square-wave}} = \sum_{m=1,3}^{k} \frac{4\Delta E}{m\pi} \sin(m\omega t), \tag{25}$$

and the amplitude $(4\Delta E/m\pi)$ of each component $(m\omega t)$ clearly becomes smaller as m increases.

Figure 6 provides a comparison of $I_p(\omega t)$ values obtained from the designer waveform, the conventional constant amplitude sinusoidal waveform and the square wave methods of FT-ac voltammetry for oxidation of 0.404 mM FcMeOH at a GC electrode, as a function of frequency. Only $I_p(\omega t)$ values obtained from the designer waveform are independent of frequency for a reversible process, allowing ready assignment of very fast electrode kinetics. $I_p(\omega t)$ values obtained from the square-wave decrease with frequency as expected, while from a multi-frequency, fixed 15 mV amplitude voltammetric experiment, $I_p(\omega t)$ increases with frequency, also as expected (approximately square root dependency).

3.5 Application of the designer waveform to other processes

A more limited set of experiments were also undertaken with the designer waveform on the reduction of 0.300 mM $[Ru(NH_3)_6]^{3+}$ and 0.300 mM $[Fe(CN)_6]^{3-}$ in aqueous 0.50 M KCl electrolyte. As for oxidation (the $[FcMeOH]^{0/+}$ process), the one-electron reduction of $[Ru(NH_3)_6]^{3+}$ to $[Ru(NH_3)_6]^{2+}$ is believed to involve a fast outer-sphere reversible electron-transfer process [4, 16]. For this process, $I_p(\omega t)$ values of background-corrected fundamental harmonic currents are close to constant at GC, platinum and gold electrodes. In this case, essentially identical background currents were obtained before and after $[Ru(NH_3)_6]^{3+}$ addition to 0.50 M KCl, implying that, adsorption is absent at all three electrode surfaces. Simulations based on a reversible process confirm that the reaction can be regarded as being very close to reversible with frequencies up to almost 2 kHz ($k^0 \geq 1$ cm s^{-1}).

A very different dependence of $I_p(\omega t)$ on frequency is found for the reduction of $[Fe(CN)_6]^{3-}$ at a GC electrode in aqueous 0.50 M KCl electrolyte (Figure 7). Data obtained at Pt or Au electrodes have quasi-reversible characteristics similar to those at GC electrodes. Comparison of background currents before and after the addition of $[Fe(CN)_6]^{3-}$ to 0.50 M KCl electrolyte suggest adsorption is minimal at all three electrode surfaces.

Simulations of a quasi-reversible process using $D = 7.6 \times 10^{-6}$ cm^2 s^{-1}; $R_u = 0$ Ω, $C_{dl} = 0.15$ Fm^{-2}; $E^{o'} = 0.278$ V, $k_0^{'} = 0.023$ cm s^{-1} and $\alpha = 0.5$, provided an excellent fit to experimental $I_p(\omega t)$ values (Figure 8). Clearly, the designer waveform can be used to show departure from reversibility and then to estimate kinetic parameters for a quasi-reversible electrochemical system.

Experiments have also been carried out with the designer waveform for oxidation of FcMeOH at a glassy carbon electrode in the very high resistance dichloromethane (0.10 M Bu_4NPF_6) medium. The FT-ac data obtained are shown in Figure 9(a). Simulations using parameters $R_u = 1100$ Ω, $C_{dl} = 0.13$ Fm^{-2}, $E^{o'} = -0.154$ V, with reversible electrode kinetics ($k_0^{'} = 10,000$ cm s^{-1}; and $\alpha = 0.5$) agree well with experimental data. Although the resistance of

this medium is high, the oxidation of FcMeOH is shown to remain reversible, as found in aqueous media. However, in this case, $I_p(\omega t)$ is not independent of frequency because of the significant contribution of the IR_u drop. In this case, direct proof of reversibility is not possible via casual inspection the plot of $I_p(\omega t)$ versus frequency. However, before assuming a process is quasi-reversible rather than reversible, studies on the concentration dependence and simulations that take R_u into account must be employed.

4 Conclusions

A multi-frequency, variable amplitude 'designer waveform' consisting of eight sine waves of amplitude from 20 mV to about 2 mV with frequencies covering the range 35 to 1970 Hz has been developed to facilitate rapid assessment of the reversibility or otherwise of electrode processes by FT-ac voltammetry. With this waveform, $I_p(\omega t)$ for the fundamental harmonic of a reversible process is predicted to be independent of frequency, provided the influence of the IR_u drop is insignificant. Reversible oxidation of ferrocenemethanol (FcMeOH), reversible reduction of hexaminеruthenium ($[Ru(NH_3)_6]^{3+}$) and the quasi-reversible reduction of ferricyanide ($[Fe(CN)_6]^{3-}$) in aqueous 0.50 M KCl electrolyte have been studied at glassy carbon, gold and platinum electrodes in order to assess the attributes of the new waveform. A major advantage of the method was found to be ready access to efficient methods for obtaining and analysing large amounts of information generated from a single experiment. Analysis of both experimental and simulated data reveals the readily recognised patterns of behaviour that enable identification of reversibility or quasi-reversibility, and contributions from uncompensated resistance and background capacitance. Excellent agreement between experimental and simulated ac voltammograms was obtained for all processes examined in aqueous 0.50 M KCl electrolyte. Provided attention is paid to the IR_u drop, the waveform can also be used to confirm that oxidation of FcMeOH is reversible in highly resistive dichloromethane solvent.

5 Acknowledgements

Financial support from the Australian Research Council is gratefully acknowledged.

6 Supplementary Material

Figures S-1 to S-4 contain ac voltammetric data. Supplementary material associated with this article can be found, in the online version, at doi:XXX

References

[1] S. O. Engblom, J. C. Myland, and K. B. Oldham. Must ac voltammetry employ small signals? *J. Electroanal. Chem.*, 480:120, 2000.

[2] D. J. Gavaghan and A. M. Bond. A complete numerical simulation of the techniques of alternating current linear sweep and cyclic voltammetry: analysis of a reversible process by conventional and fast Fourier transform methods. *J. Electroanal. Chem.*, 480:133, 2000.

[3] D. E. Smith. *Electroanalytical Chemistry: A Series of Advances*, volume 1. Marcal Dekker, New York, 1966.

[4] J. Zhang, S. Guo, and A. M. Bond. Large amplitude Fourier transformed high-harmonic alternating current cyclic voltammetry: kinetic discrimination of interferring faradaic processes at glassy carbon and at boron doped diamond electrodes. *Anal. Chem.*, 76:3619, 2004.

[5] S. Guo, J. Zhang, D. Elton, and A. M. Bond. Fourier transform large-amplitude alternating current cyclic voltammetry of surface-bound azurin. *Anal. Chem.*, 76:166, 2004.

[6] B. Lertanantawong, A. P. O'Mullane, J. Zhang, W. Surareungchai, M. Somasundrum, and A. M. Bond. Investigation of mediated oxidation of ascorbic acid by ferrocenemethanol using large-amplitude Fourier transformed ac voltammetry under quasi-reversible electron-transfer conditions at an indium tin oxide electrode. *Anal. Chem.*, 80:6515, 2008.

[7] D. J. Gavaghan, D. M. Elton, and A. M. Bond. Numerical simulation of alternating current linear sweep voltammetry at microdisc electrodes. *Collect. Czech. Chem. Commun.*, 66:255, 2001.

[8] D. J. Gavaghan, D. Elton, and A. M. Bond. A comparison of sinusoidal, square wave, sawtooth, and staircase forms of transient ramped voltammetry when a reversible process is analysed in the frequency domain. *J. Electroanal. Chem.*, 513:73, 2001.

[9] D. J. Gavaghan, D. Elton, K. B. Oldham, and A. M. Bond. Analysis of

ramped square-wave voltammetry in the frequency domain. *J. Electroanal. Chem.*, 512:1, 2001.

[10] M. Rosvall and M. Sharp. A complete system for electrochemical impedance spectroscopy which combines FFT methods and staircase voltammetry. *Electrochem. Commun.*, 2:338, 2000.

[11] J. Hàzí, D. M. Elton, W. A. Czerwinski, V. A. Vicente-Beckett, and A. M. Bond. Microcomputer-based instrumentation for multi-frequency Fourier transform alternating current (admittance and impedance) voltammetry. *J. Electroanal. Chem.*, 437:1, 1997.

[12] J. Schiewe, J. Hàzí, V. A. Vicente-Beckett, and A. M. Bond. A unified approach to trace analysis and evaluation of electrode kinetics with fast Fourier transform electrochemical instrumentation. *J. Electroanal. Chem.*, 451:129, 1998.

[13] A. M. Bond, N. W. Duffy, S. Guo, J. Zhang, and D. Elton. Changing the look of voltammetry. Can FT revolutionize voltammetric techniques as it did for NMR? *Anal. Chem.*, 77:186A, 2005.

[14] M. P. Longinotti and H. R. Corti. Diffusion of ferrocene methanol in supercooled aqueoue solutions using cylindrical microelectrodes. *Electrochem. Commun.*, 9:1444, 2007.

[15] C. Cannes, F. Kanoufi, and A. J. Bard. Cyclic voltammetry and scanning electrochemical microscopy of ferrocenemethanol at monolayer and bilayer-modified gold electrodes. *J. Electroanal. Chem.*, 547:83, 2003.

[16] M. Pyo and A. J. Bard. Scanning electrochemical microscopy. 35. Determination of diffusion coefficients and concentrations of $Ru(NH_3)_6^{3+}$ and methylene blue in polyacrylamide films by chronoamperometry at ultramicrodisk electrodes. *Electrochim. Acta*, 42:3077, 1997.

[17] A. J. Bard and L. R. Faulkner. *Electrochemical Methods*. Wiley, New York, 2nd edition, 2001.

[18] D. J. Gavaghan and A. M. Bond. Numerical simulation of the effects of

experimental error on the higher harmonic components of Fourier transformed ac voltammetry. *Electroanal*, 18:333, 2006.

[19] K. W. Morton and D. F. Mayers. *Numerical Solution of Partial Differential Equations*. Cambridge University Press, Cambridge, 1994.

[20] R. Brent. *Algorithms for Minimization without Derivatives*. Prentice Hall, England, 1973.

[21] A. A. Sher, A. M. Bond, D. J. Gavaghan, K. Harriman, S. W. Feldberg, and N. W. Duffy. Resistance, capacitance, and electrode kinetic effects in Fourier-transformed large-amplitude sinusoidal voltammetry: emergence of powerful and intuitively obvious tools for recognition of patterns of behaviour. *Anal. Chem.*, 76:6214, 2004.

[22] A. M. Bond. *Modern Polarographic Methods in Analytical Chemistry*. Marcal Dekker, New York, 1980.

[23] A. A. Sher, A. M. Bond, D. J. Gavaghan, K. Gillow, N. W. Duffy, S. Guo, and J. Zhang. Fourier transformed large amplitude square-wave voltammetry as an alternative to impedance spectroscopy: Evaluation of resistance, capacitance and electrode kinetic effects via an heuristic approach. *Electroanal.*, 17:1450, 2005.

Figure Legends

Figure 1. (a) Raw *I-t* data obtained at a GC electrode for oxidation of 0.404 mM FcMeOH in 0.5 M KCl. (b) 1:8 decimated data. (c) Power spectrum obtained after FT. (d)–(m) i-FT-recovered dc, 1st, 2nd and 3rd harmonic responses (only those derived from sine waves at 34.94 Hz, 370.00 Hz and 1970.01 Hz) are shown.

Figure 2. (a) Raw *I-t* data obtained at a GC electrode for oxidation of 0.404 mM FcMeOH in 0.5 M KCl. (b) FT-recovered 1st harmonic for all eight component frequencies. (c) 1:8 decimated data. (d) FT-recovered fundamental harmonics from 1:8 decimated ac voltammogram for all eight component frequencies. (e) Decimated and background current corrected data. (f) FT-recovered fundamental harmonic responses from 1:8 decimated data and background current corrected ac voltammogram for all frequencies.

Figure 3. Background corrected $I_p(\omega t)$ vs frequency data obtained from FT-ac voltammetry at a GC electrode for oxidation of designated FeMeOH concentrations in 0.50 M KCl.

Figure 4. (a) FT-recovered fundamental harmonic ac voltammograms simulated for a reversible process with, $R_u = 100\ \Omega$ and $C_{\rm dl} = 0\ {\rm Fm}^{-2}$. Other parameters used in simulation are as for Figure S-1. (b) Experimental and simulated data (0.50 M KCl with 0.404 mM FcMeOH) illustrating the influence of uncompensated resistance.

Figure 5. Comparison of I_p versus frequency data obtained from oxidation of 0.404 mM FcMeOH at a glassy carbon electrode in 0.50 M KCl using the designer variable amplitude waveform in one experiment versus using eight individual single-frequency measurements. Faradaic currents in both cases were corrected using the baseline-subtraction method.

Figure 6. $I_p(\omega t)$ values from oxidation of 0.4 mM FcMeOH in 0.50 M KCl at a glassy carbon electrode from FT-recovered fundamental harmonics as a function of frequency using the new designer waveform, fixed 15 mV

amplitude and square wave voltammetry.

Figure 7. (a) Raw I-t data obtained using the multi-time scale method for reduction of 0.300 mM $[Fe(CN)_6]^{3-}$ in 0.50 M KCl at a GC electrode. (b)-(i) FT-ac recovered fundamental harmonics for each frequency in I-t format. (j) FT-ac recovered 1st harmonics for all eight component frequencies in 'envelope' I_{amp}-t format.

Figure 8. (a) Simulated fundamental ac harmonics mimicking experimental data in Figure 7(j) in I_{amp} format. (b) Comparison of $I_p(\omega t)$ values obtained from experimental data and by simulation after background correction. Simulation parameters are provided in the text.

Figure 9. (a) Fundamental harmonic FT-ac voltammograms displayed in I_{amp}-t format for oxidation of 0.400 mM FeMeOH in dichloromethane (0.10 mM Bu_4NPF_6) at a GC electrode. (b) Simulated FT-ac voltammograms. (c) Comparison of experimental and simulated $I_p(\omega t)$ values before and after background correction.

Tables

Component	Frequency (Hz)	Amplitude (mV)
1	34.94	20.00
2	89.97	12.46
3	229.96	7.79
4	370.00	6.14
5	589.97	4.86
6	929.94	3.88
7	1369.98	3.19
8	1970.01	2.66

Table 1: Sine-wave components used in the composite designer waveform FT-ac voltammetric experiments. The dc potential range chosen for oxidation of FcMeOH in 0.50 M KCl is 0–500.00 mV vs. Ag | AgCl (selected 500 mV range chosen in other cases); the dc scan rate is 37.25 mVs^{-1}; the total number of data points collected is 2^{18}. Note that the choice of applied potential for each sine wave in this designer waveform is based on the relationship $\Delta E_i \propto \sqrt{\omega_i}$.

Figures

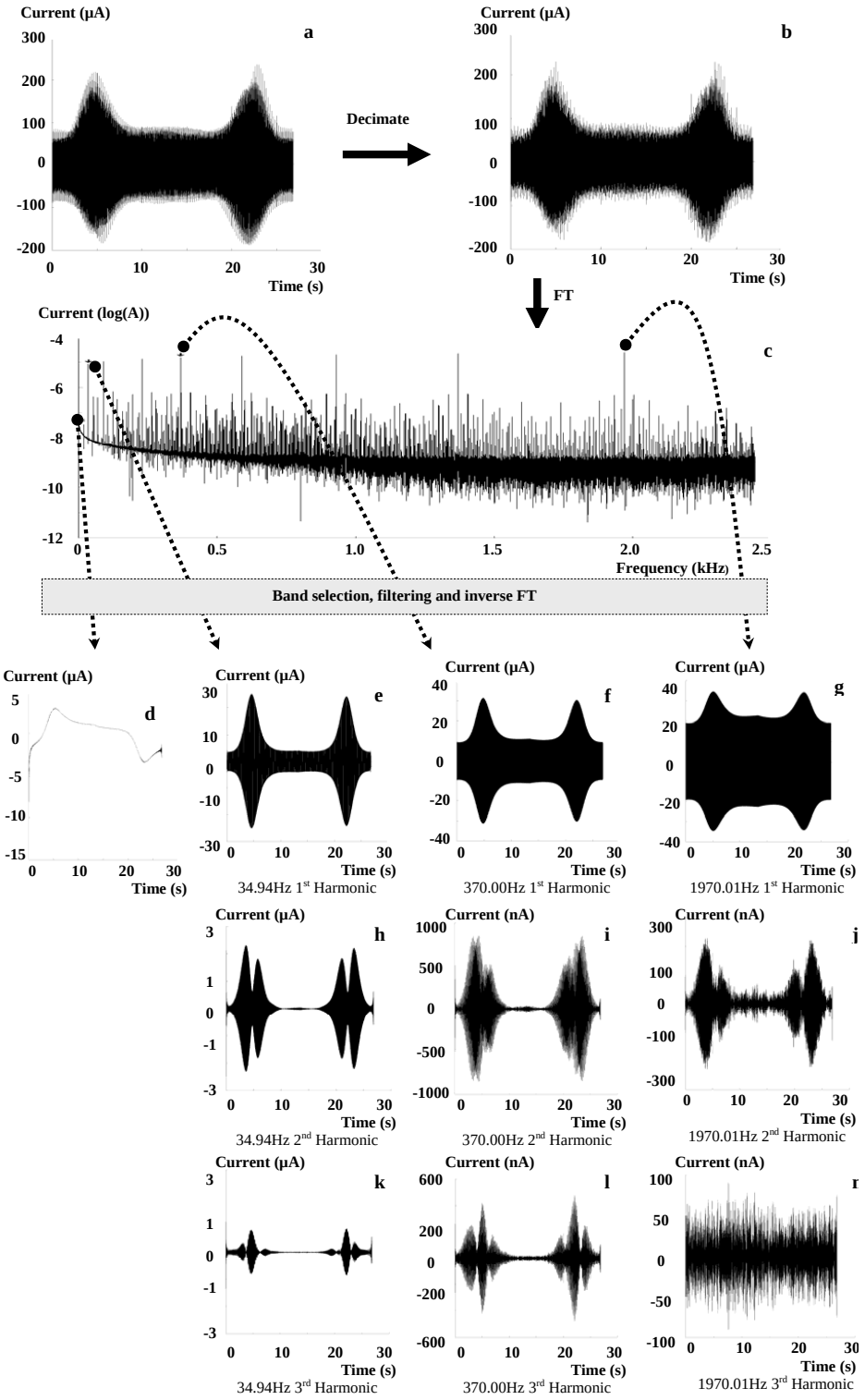
Current (μA)
a
Time (s)
Decimate
Current (μA)
b
Time (s)
FT
Current (log(A))
c
Frequency (kHz)
Band selection, filtering and inverse FT
Current (μA)
d
Time (s)
Current (μA)
e
Time (s)
34.94Hz 1st Harmonic
Current (μA)
f
Time (s)
370.00Hz 1st Harmonic
Current (μA)
g
Time (s)
1970.01Hz 1st Harmonic
Current (μA)
h
Time (s)
34.94Hz 2nd Harmonic
Current (nA)
i
Time (s)
370.00Hz 2nd Harmonic
Current (nA)
j
Time (s)
1970.01Hz 2nd Harmonic
Current (μA)
k
Time (s)
34.94Hz 3rd Harmonic
Current (nA)
l
Time (s)
370.00Hz 3rd Harmonic
Current (nA)
r
Time (s)
1970.01Hz 3rd Harmonic

Figure 1:

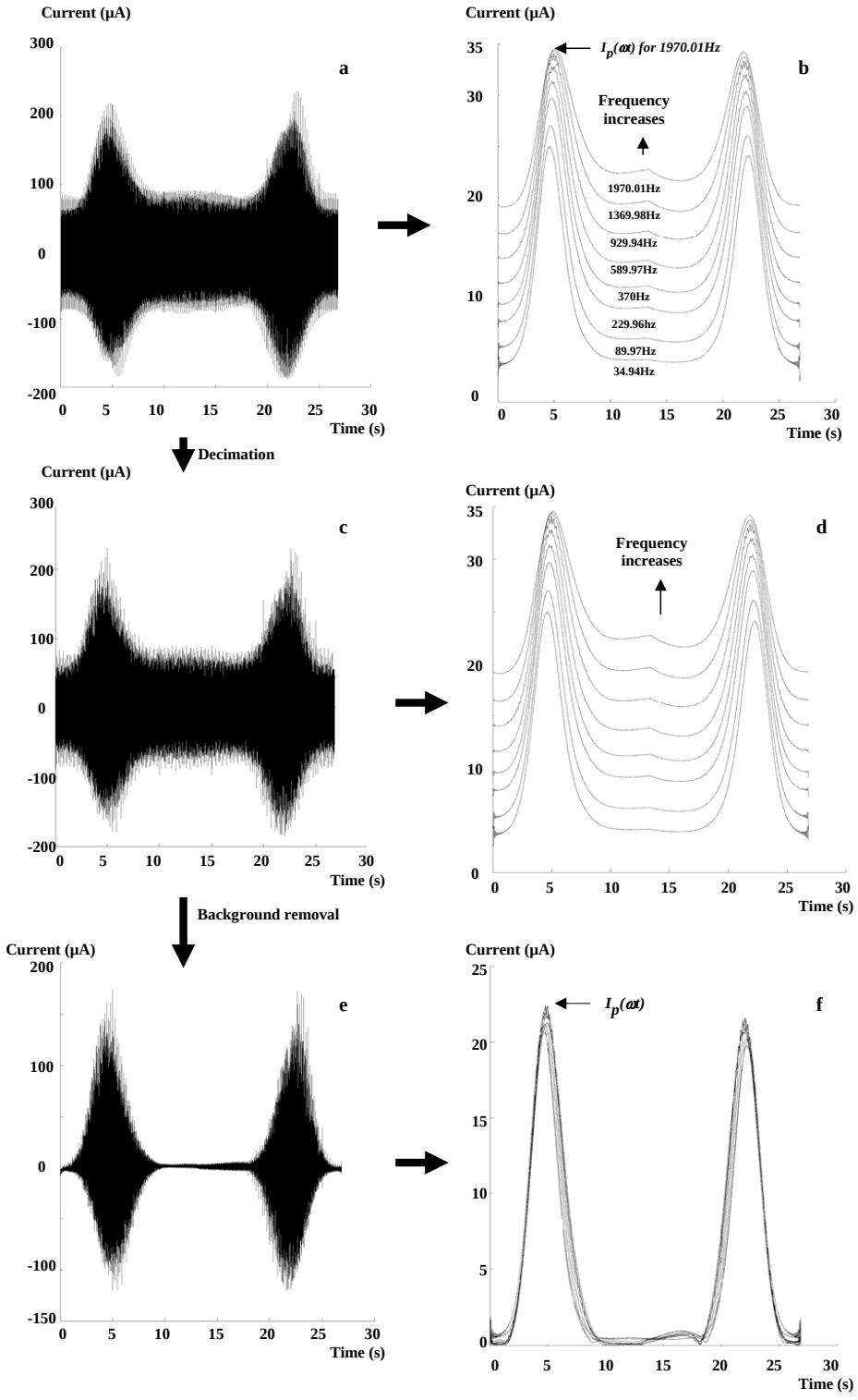
Current (μA)
a
Time (s)
Current (μA)
b
$I_p(\omega t)$ for 1970.01Hz
Frequency increases
1970.01Hz
1369.98Hz
929.94Hz
589.97Hz
370Hz
229.96hz
89.97Hz
34.94Hz
Time (s)
Decimation
Current (μA)
c
Time (s)
Current (μA)
d
Frequency increases
Time (s)
Background removal
Current (μA)
e
Time (s)
Current (μA)
f
$I_p(\omega t)$
Time (s)

Figure 2:

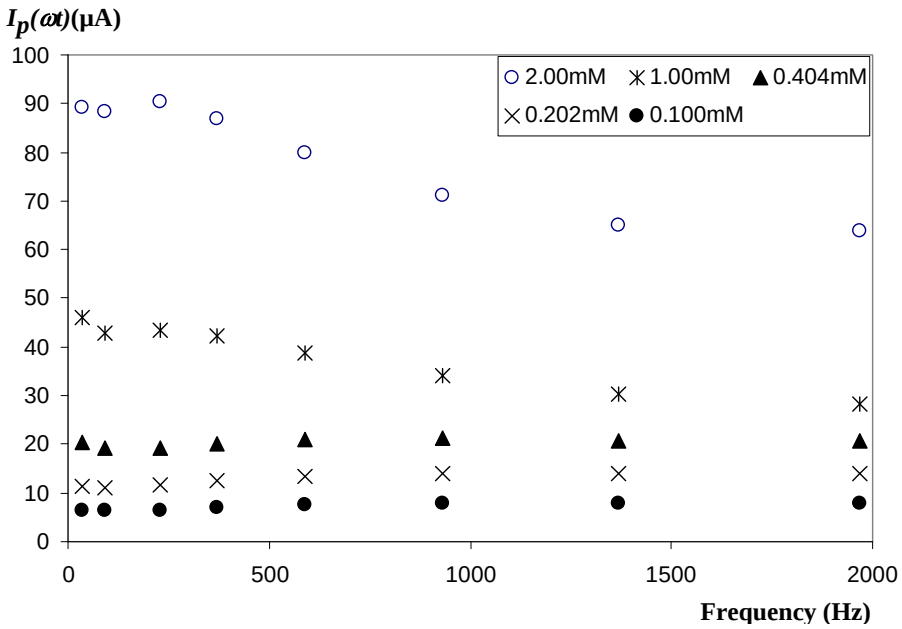
$I_p(\omega t)$(μA)
100
90
80
70
60
50
40
30
20
10
0
0
500
1000
1500
2000
Frequency (Hz)
2.00mM
1.00mM
0.404mM
0.202mM
0.100mM

Figure 3:

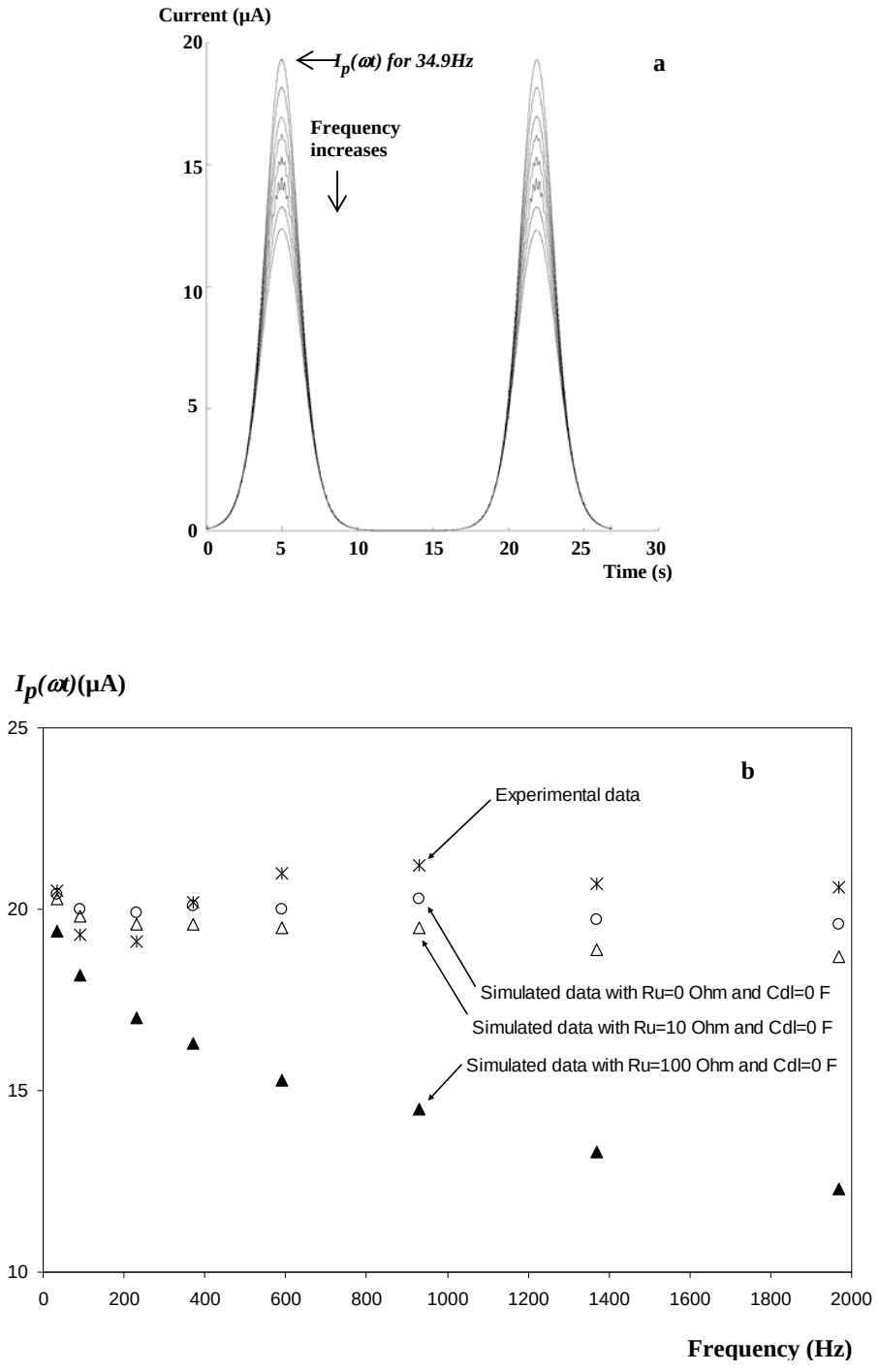
Current (μA)
20
15
10
5
0
$I_p(\omega t)$ for 34.9Hz
a
Frequency increases
0
5
10
15
20
25
30
Time (s)
$I_p(\omega t)$(μA)
25
20
15
10
b
Experimental data
Simulated data with Ru=0 Ohm and Cdl=0 F
Simulated data with Ru=10 Ohm and Cdl=0 F
Simulated data with Ru=100 Ohm and Cdl=0 F
0
200
400
600
800
1000
1200
1400
1600
1800
2000
Frequency (Hz)

Figure 4:

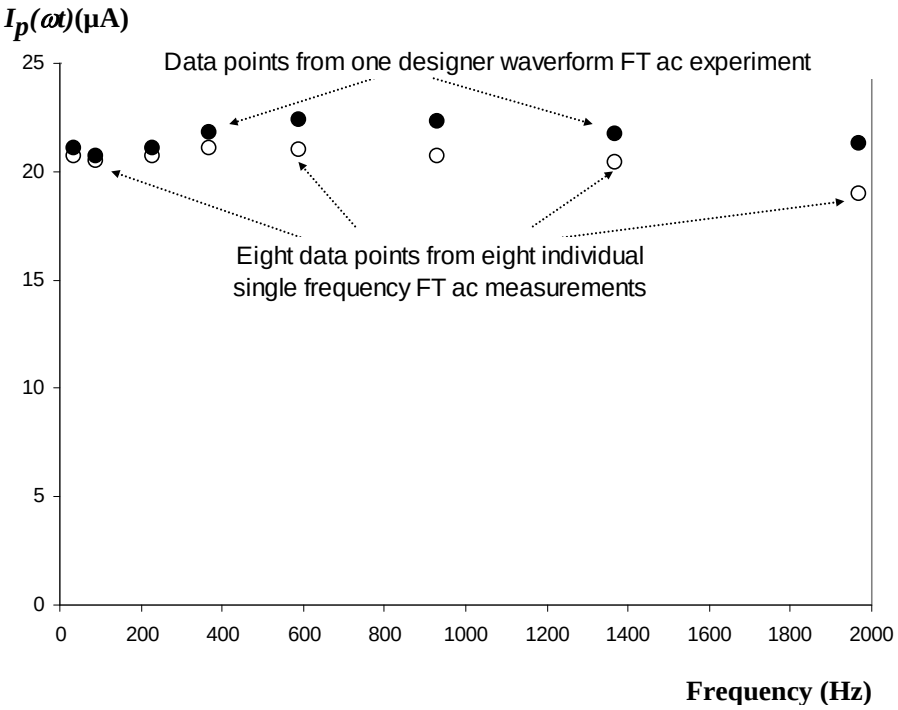
$I_p(\omega t)$(μA)
Data points from one designer waverform FT ac experiment
Eight data points from eight individual
single frequency FT ac measurements
25
20
15
10
5
0
0
200
400
600
800
1000
1200
1400
1600
1800
2000
Frequency (Hz)

Figure 5:

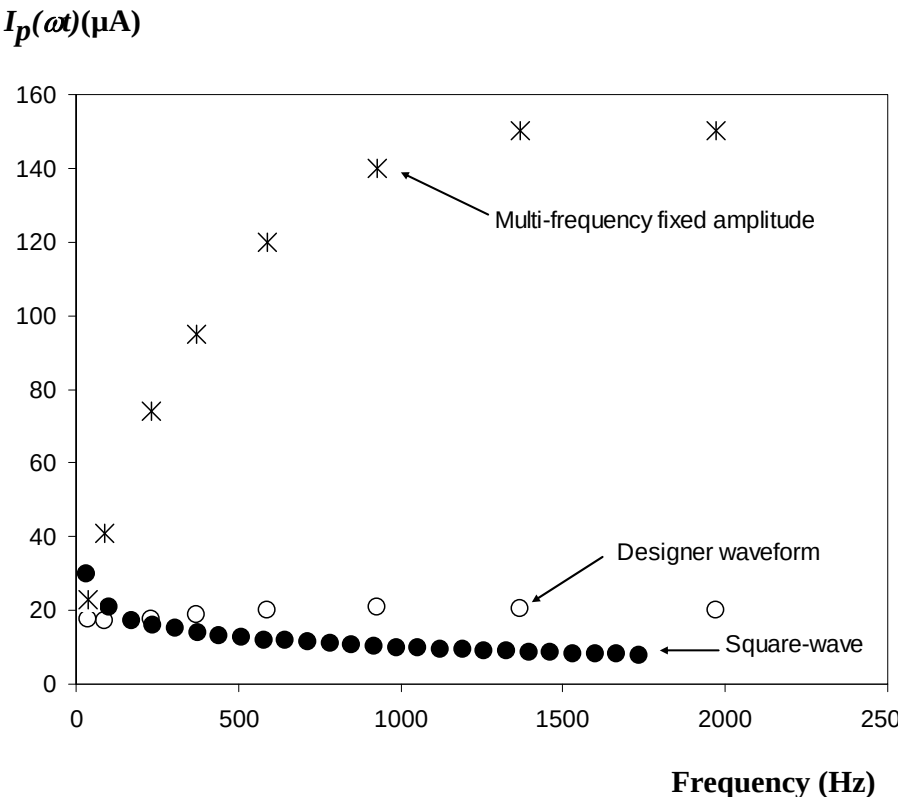
$I_p(\omega t)$(μA)
160
140
120
100
80
60
40
20
0
0
500
1000
1500
2000
250
Multi-frequency fixed amplitude
Designer waveform
Square-wave
Frequency (Hz)

Figure 6:

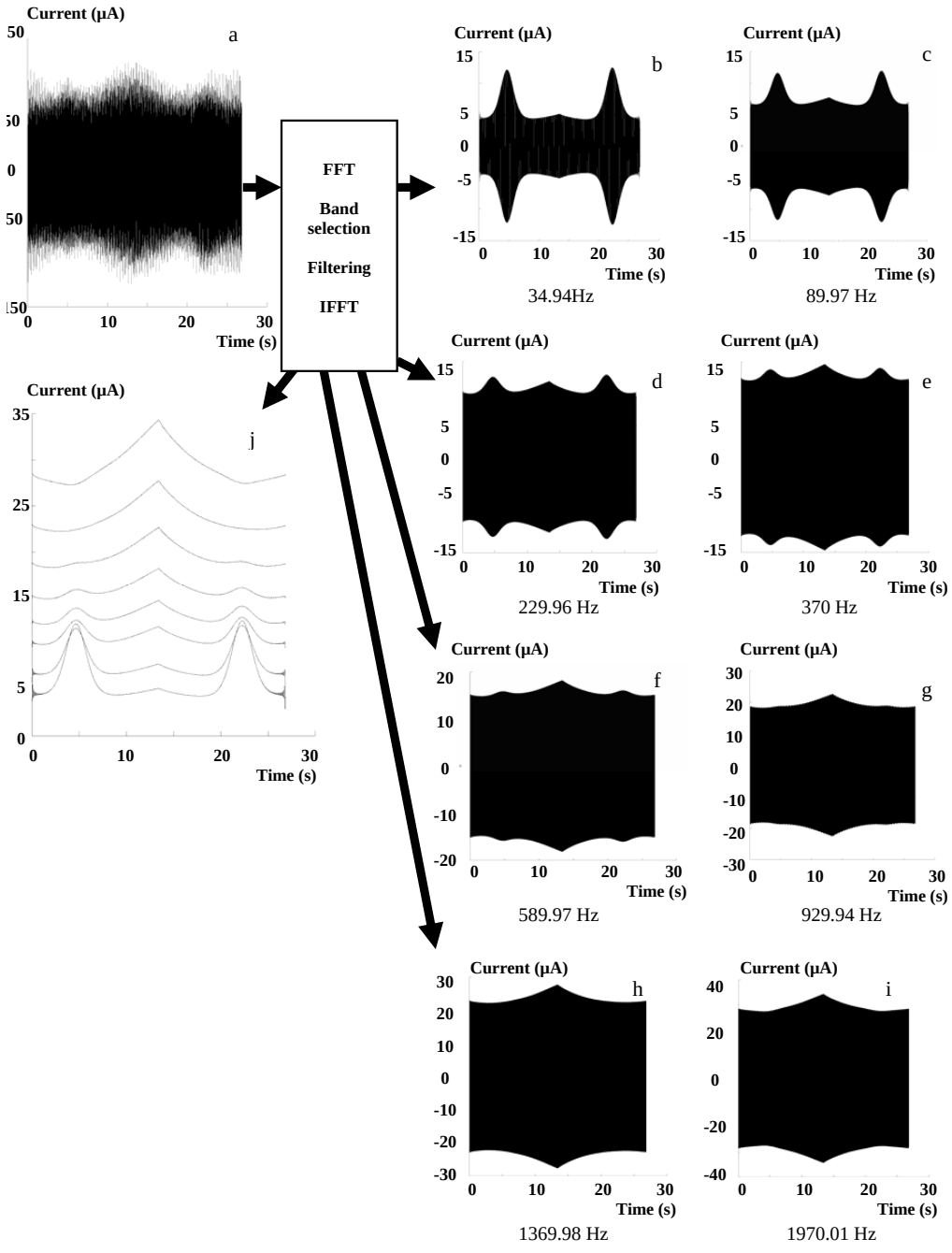
Current (μA)
a
Time (s)
FFT
Band selection
Filtering
IFFT
Current (μA)
b
Time (s)
34.94Hz
Current (μA)
c
Time (s)
89.97 Hz
Current (μA)
d
Time (s)
229.96 Hz
Current (μA)
e
Time (s)
370 Hz
Current (μA)
f
Time (s)
589.97 Hz
Current (μA)
g
Time (s)
929.94 Hz
Current (μA)
h
Time (s)
1369.98 Hz
Current (μA)
i
Time (s)
1970.01 Hz
Current (μA)
j
Time (s)

Figure 7:

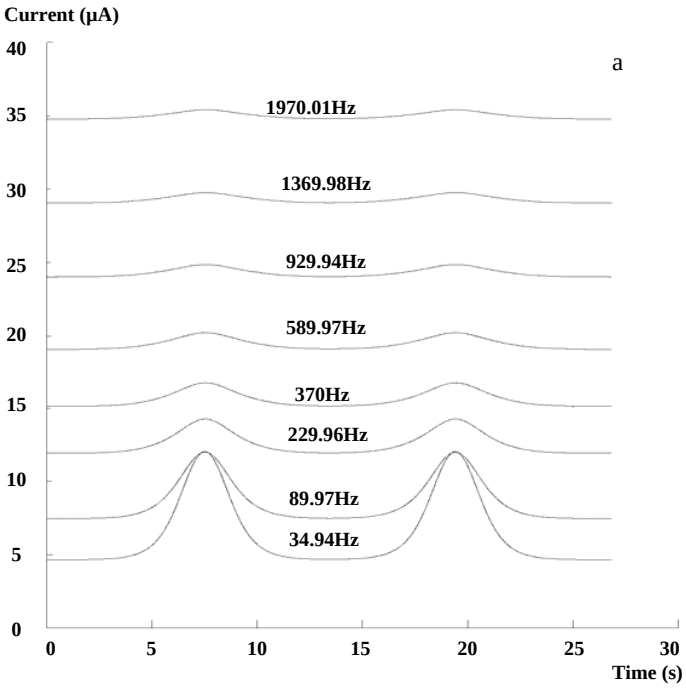
Current (μA)
a
1970.01Hz
1369.98Hz
929.94Hz
589.97Hz
370Hz
229.96Hz
89.97Hz
34.94Hz
Time (s)

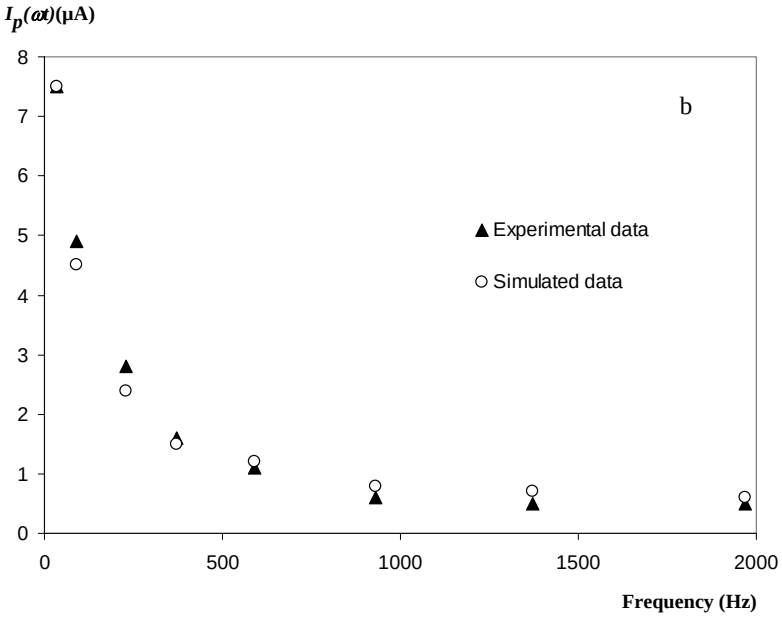
$I_p(\omega t)$(μA)
b
Experimental data
Simulated data
Frequency (Hz)

Figure 8:

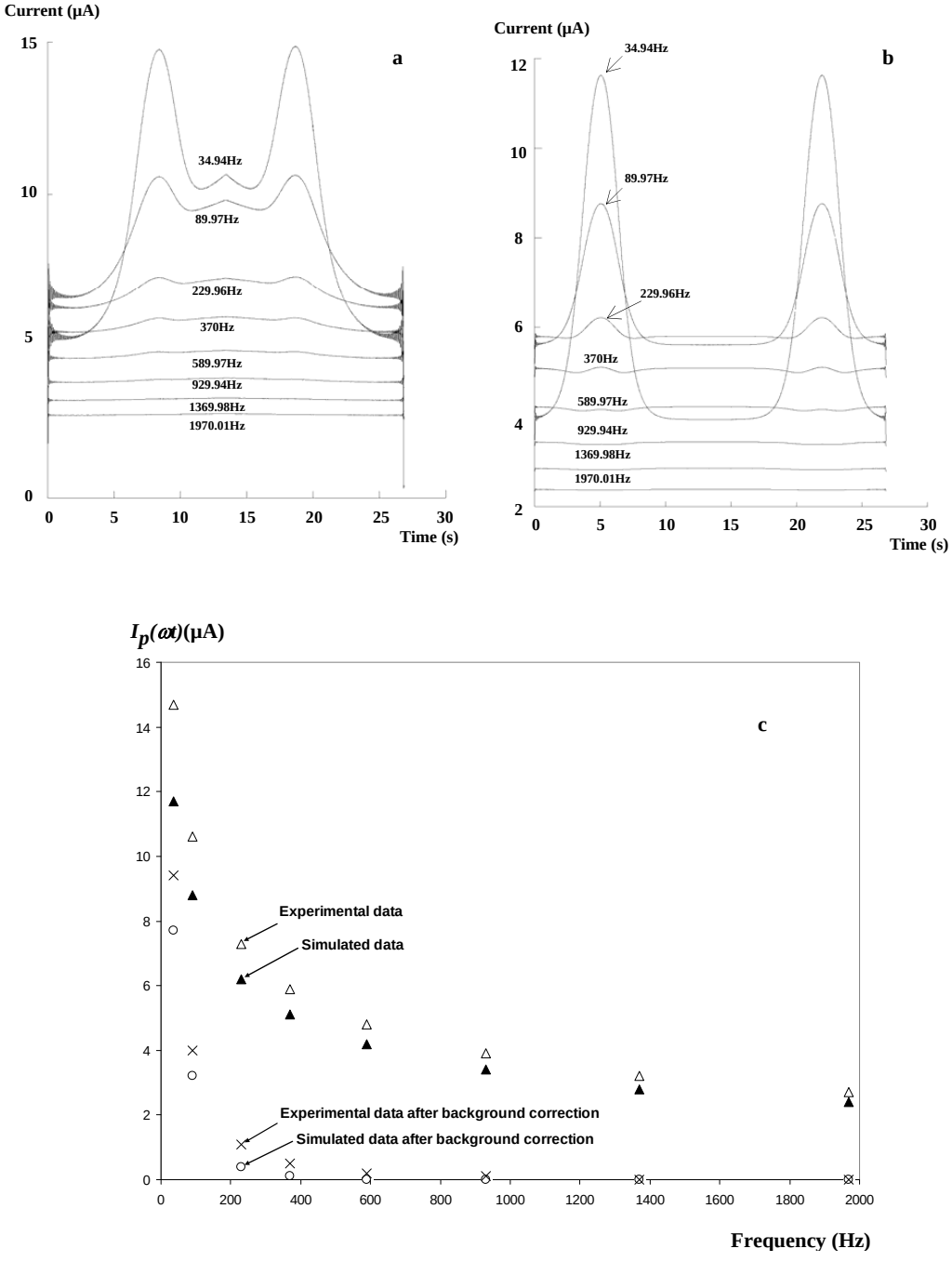
Current (μA)
a
34.94Hz
89.97Hz
229.96Hz
370Hz
589.97Hz
929.94Hz
1369.98Hz
1970.01Hz
Time (s)
Current (μA)
b
34.94Hz
89.97Hz
229.96Hz
370Hz
589.97Hz
929.94Hz
1369.98Hz
1970.01Hz
Time (s)
$I_p(\omega t)$(μA)
c
Experimental data
Simulated data
Experimental data after background correction
Simulated data after background correction
Frequency (Hz)

Figure 9:

Supplementary Material for Designer Based Fourier Transformed Voltammetry: A Multi-frequency, Variable Amplitude, Sinusoidal Waveform

Yongjun Tan[a, 1] Gareth P. Stevenson[b] Ruth E. Baker[c]
Darrell Elton[d] Kathryn Gillow[b] Jie Zhang[e]
Alan M. Bond[a, *] David J. Gavaghan[b, *]

[a]School of Chemistry, Monash University, Clayton, Melbourne, Victoria 3800, Australia.

[b]Oxford University Computing Laboratory, Wolfson Building, Parks Road, Oxford, OX1 3QD, United Kingdom.

[c]Centre for Mathematical Biology, Mathematical Institute, 24-29 St. Giles', Oxford OX1 3LB, United Kingdom.

[d]Department of Electronic Engineering, Latrobe University, Bundoora, Victoria 3083, Australia.

[e]Institute of Bioengineering and Nanotechnology, 31 Biopolis Way, The Nanos, Singapore 138669.

[1]Present address: School of Applied Chemistry, Curtin University of Technology, Perth, Australia.

[*]Corresponding authors. Alan M. Bond, email: Alan.Bond@sci.monash.edu.au, telephone: +61 3 9905 1338, fax: +61 3 9905 4597. David J. Gavaghan, email: David.Gavaghan@comlab.ox.ac.uk, telephone: +44 1865 610667, fax: +44 1865 610670.

Supplementary Figure Legends

Figure S-1. (a) I-t data simulated to mimic experimental data displayed in 2(a). (b) FT-recovered fundamental harmonics simulated to mimic experimental data displayed in Figure 2(b). Parameters used in simulation of a reversible process are provided in the text.

Figure S-2. (a) I-t, (b) fundamental harmonic, data simulated with zero background current in order to mimic experimental data displayed in Figure 2(e) and (f). Parameters used to simulate the reversible process are provided in the text and as for Figure S-1 except $C_{\mathrm{dl}} = 0$ Fm^{-2}.

Figure S-3. Comparison of fundamental harmonic background currents before and after addition of FcMeOH. (a) $I(\omega t)$ versus t data at GC electrode in 0.5 M KCl. (b) as for (a) but after addition of 2.0 mM FcMeOH. (c) Comparison of fundamental harmonic background currents before and after FcMeOH addition.

Figure S-4. (a) Raw current versus time data obtained when 0.100 mM FcMeOH is oxidised at a GC electrode in 0.50 M KCl electrolyte. (b and c) Background corrected current using different designated time regimes: (b) with 0.5-1.5 and 11-12 s, and (c) with 0-1 and 10-11 s correction reference zones.

Supplementary Figures

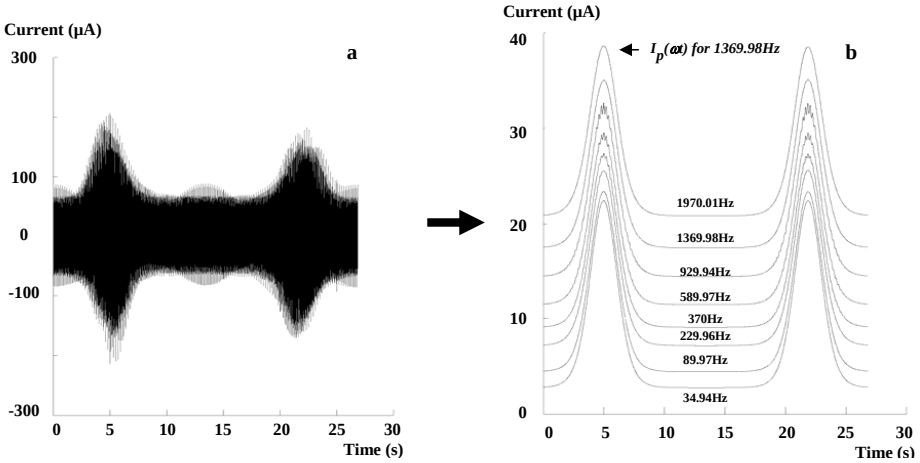

Figure S-1:

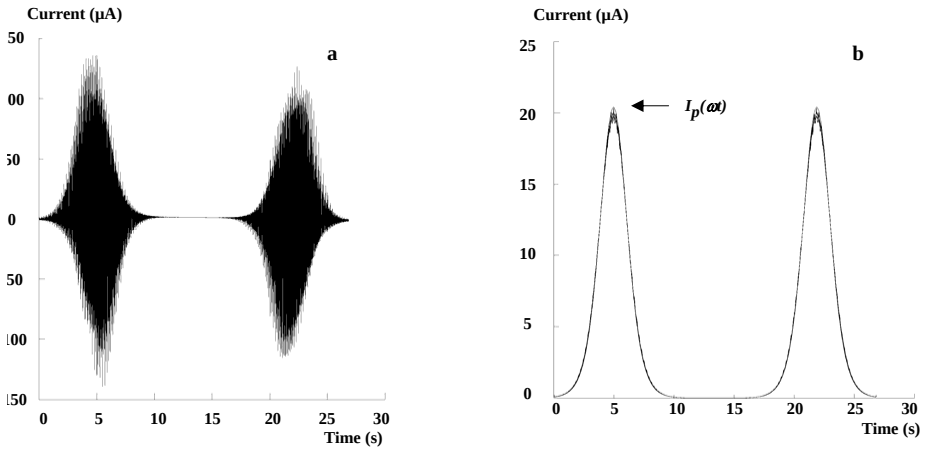

Figure S-2:

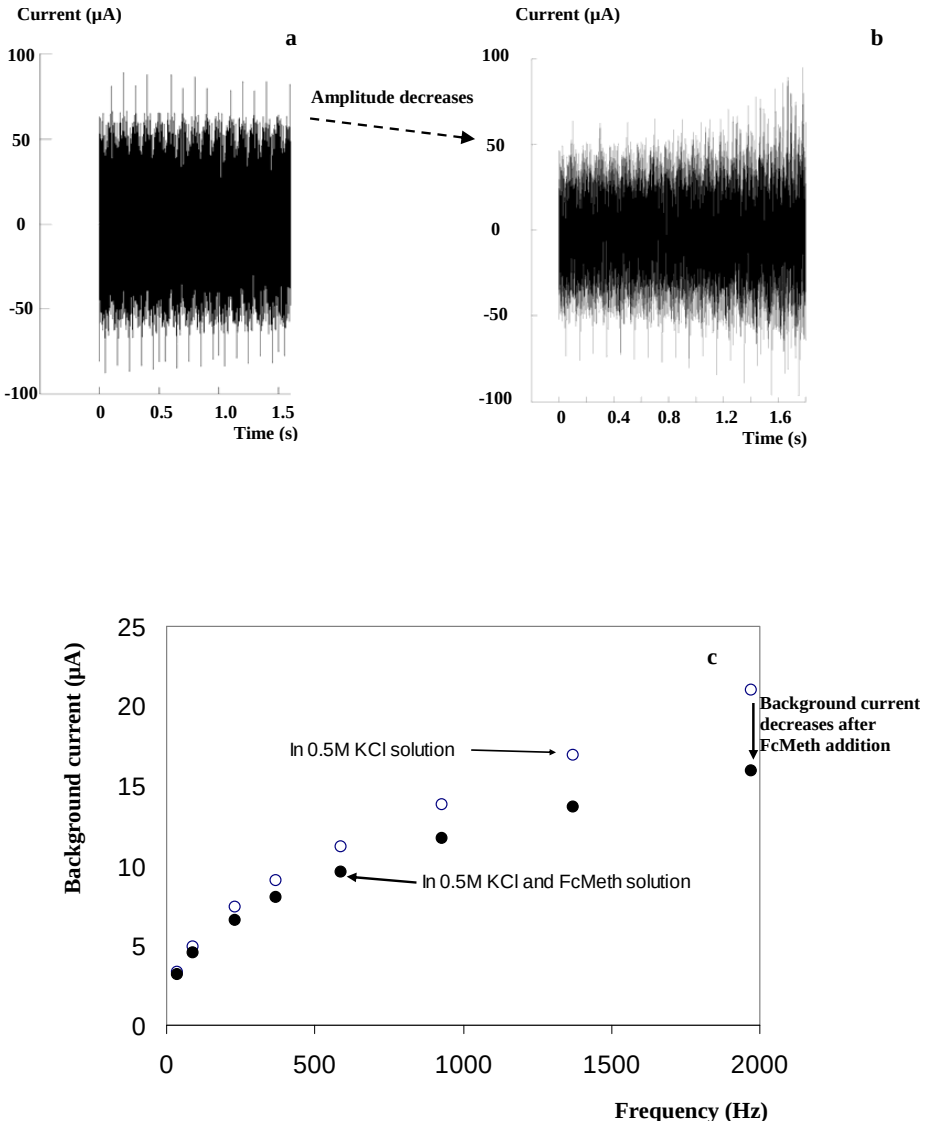
Current (µA)
a
100
50
0
-50
-100
0
0.5
1.0
1.5
Time (s)
Amplitude decreases
Current (µA)
b
100
50
0
-50
-100
0
0.4
0.8
1.2
1.6
Time (s)
c
Background current (µA)
25
20
15
10
5
0
0
500
1000
1500
2000
Frequency (Hz)
In 0.5M KCl solution
In 0.5M KCl and FcMeth solution
Background current decreases after FcMeth addition

Figure S-3:

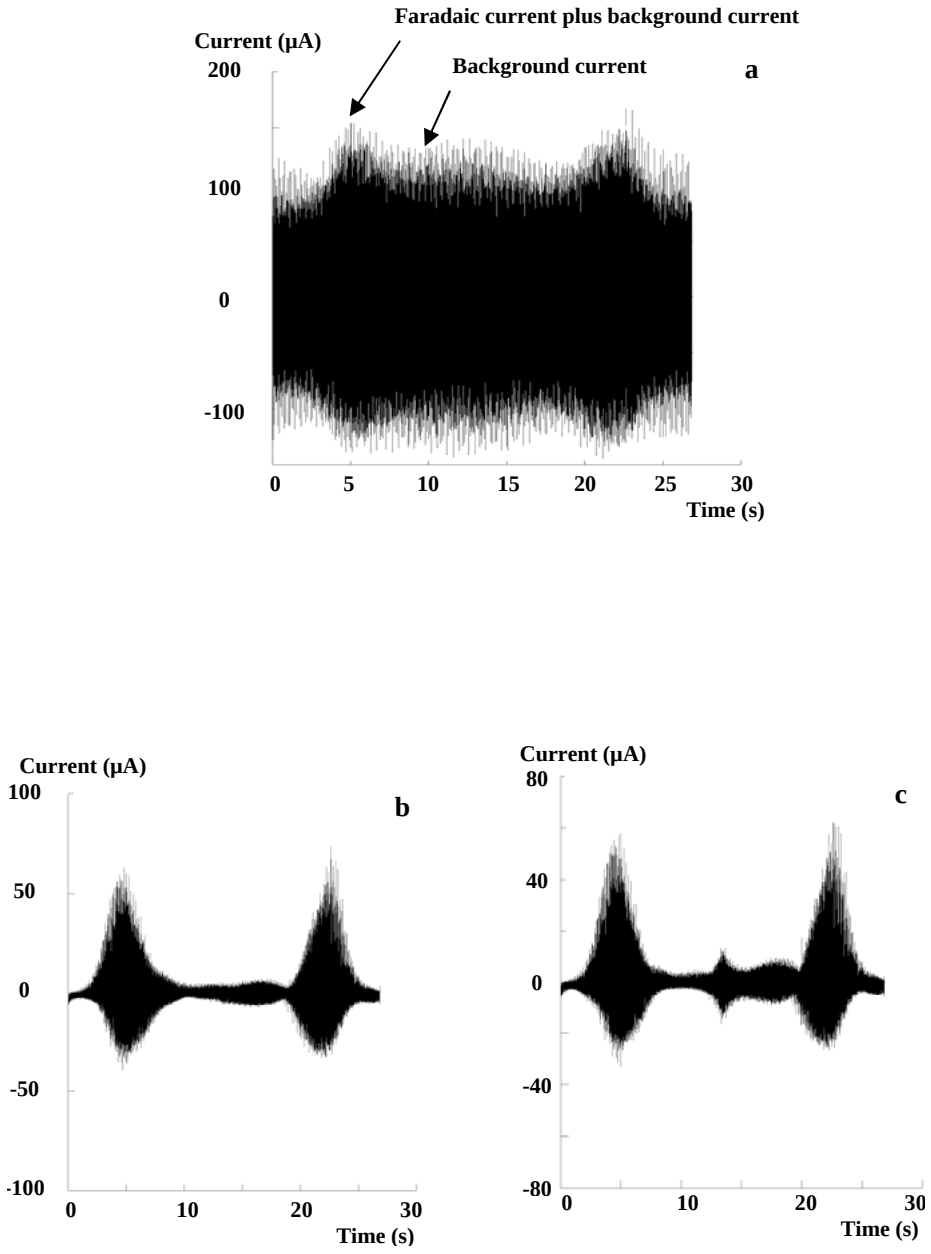
Faradaic current plus background current
Current (µA)
Background current
a
200
100
0
-100
0
5
10
15
20
25
30
Time (s)
Current (µA)
b
100
50
0
-50
-100
0
10
20
30
Time (s)
Current (µA)
c
80
40
0
-40
-80
0
10
20
30
Time (s)

Figure S-4:

Designer Based Fourier Transformed Voltammetry: A Multi-frequency, Variable Amplitude, Sinusoidal Waveform

Yongjun Tan[a, 1] Gareth P. Stevenson[b] Ruth E. Baker[c]
Darrell Elton[d] Kathryn Gillow[b] Jie Zhang[e]
Alan M. Bond[a, *] David J. Gavaghan[b, *]

[a]School of Chemistry, Monash University, Clayton, Melbourne, Victoria 3800, Australia.

[b]Oxford University Computing Laboratory, Wolfson Building, Parks Road, Oxford, OX1 3QD, United Kingdom.

[c]Centre for Mathematical Biology, Mathematical Institute, 24-29 St. Giles', Oxford OX1 3LB, United Kingdom.

[d]Department of Electronic Engineering, Latrobe University, Bundoora, Victoria 3083, Australia.

[e]Institute of Bioengineering and Nanotechnology, 31 Biopolis Way, The Nanos, Singapore 138669.

[1]Present address: School of Applied Chemistry, Curtin University of Technology, Perth, Australia.

*Corresponding authors. Alan M. Bond, email: Alan.Bond@sci.monash.edu.au, telephone: +61 3 9905 1338, fax: +61 3 9905 4597. David J. Gavaghan, email: David.Gavaghan@comlab.ox.ac.uk, telephone: +44 1865 610667, fax: +44 1865 610670.

Abstract

Fourier transform methods allow custom-designed complex waveforms to be used in ac voltammetry. Commonly a single wave or sum of sine waves of variable angular frequency (ω) but constant amplitude (ΔE) superimposed onto a dc ramp are employed. In the present case, a custom-designed waveform consisting of a combination of eight sine waves is introduced, with the property that each sine wave within the composite waveform has the property $\Delta E_i \propto 1/\sqrt{\omega_i}$ where i represents the i^{th} sine wave. Frequencies (and amplitudes) employed in a single experiment cover the range from 34.94 Hz (20 mV) to 1970.01 Hz (2.66 mV). Reversibility is readily detected via use of this designer waveform by noting a constant peak height ($I_p(\omega t)$) for all eight frequencies, whereas $I_p(\omega t)$ values decrease in a characteristic manner with increasing frequency or when uncompensated resistance is present, as demonstrated experimentally and theoretically. Importantly, background charging current contributions do not increase to a level that makes measurement of faradaic current difficult at high frequencies and hence charging current is readily corrected for over the entire frequency range of interest.

Keywords: designer ac waveform, Fourier transform voltammetry, variable amplitude and frequency.

1 Introduction

During the last decade, quantitative use of the technique of Fourier transformed (FT) ac voltammetry has been expanded [1, 2] to accommodate large levels of nonlinearity introduced by application of potential perturbations with amplitudes much larger than those customarily employed in ac voltammetry or impedance spectroscopy [3]. Typically, in these recent studies, a sinusoidal waveform of amplitude up to 200 mV with a frequency of 10 Hz–50 kHz is superimposed onto the triangular waveform used in dc cyclic voltammetry. The large amplitude method, when analysed in the frequency domain via a Fourier transform-inverse Fourier transform sequence, provides simultaneous access to the dc and fundamental harmonic ac responses, in addition to higher ac harmonics that emerge from the nonlinearity. This large-amplitude FT ac technique is advantageous in studies of electrode kinetics because of the well-defined patterns of behaviour that emerge in the now readily detected higher harmonics [4], with minimal problem from charging current. The large amplitude technique has been applied successfully to elucidate details of the electrochemistry of complex electrode processes such as surface-bound azurin [5] and mediated oxidation of acerbic acid by ferrocenemethanol [6].

Theoretical treatments for the sinusoidal version of the large-amplitude FT-ac method have been developed by Engblom and Oldham et al. [1] and Gavaghan and Bond et al. [2, 7–9]. Furthermore, recent work from several laboratories has demonstrated that instrumentation can be developed in which a periodic ac waveform of any amplitude may be superimposed onto a linear or triangular dc voltage [1, 2, 5, 8, 10]. Gavaghan et al. have also described a large amplitude FT square wave ac method that has been termed 'square-wave voltammetry in the frequency domain' [9]. Other waveforms have also been suggested that are based on the Fourier series of sawtooth or other waveforms. Custom-designed instrumentation has been developed to specifically accommodate the sinusoidal and the other variations of the FT-ac technique [11, 12].

As part of our effort to further develop the FT-ac voltammetric technique, we now introduce a multi-frequency and variable amplitude waveform. The

concept behind this initial development of a designer waveform for characterising a particular class of electrochemical processes is to identify combinations of sine waves that allow the rapid identification of the nature of charge transfer processes described by Equation (1) where $E^{o'}$ is the reversible formal potential, $k^{o'}$ is the heterogeneous charge transfer rate constant at $E^{o'}$, n is the number of electrons transferred and α is the charge transfer coefficient.

$$A + ne^- \underset{}{\overset{\alpha,\, k^{o'},\, E^{o'}}{\rightleftharpoons}} B \tag{1}$$

The waveform introduced for identifying reversibility in this paper is a combination of sine waves, with the property that each sine wave within the composite waveform has the property $\Delta E_i \propto 1/\sqrt{\omega_i}$, where ω_i and ΔE_i are the angular frequency and the amplitude of the i^{th} sine wave respectively. The concept is based on the analytical solution available in small amplitude ac voltammetry when a single sine wave is applied, under conditions of planar diffusion,

$$I(\omega t) = \frac{n^2F^2Ac_A(\omega D_A)^{\frac{1}{2}}\Delta E}{4RT\cosh^2\left(\frac{j}{2}\right)}\sin\left(\omega t + \frac{\pi}{4}\right), \tag{2}$$

where A is the electrode area, c_A is the concentration of species A, n is the number of electrons transferred ($n = 1$ in the present case), D_A is the diffusion coefficient of species A, t is time, $j = nF(E_{\text{dc}} - E^{o'})/RT$ and E_{dc} is the dc component of the applied potential, $E_{\text{dc}} = E_{\text{initial}} + vt$, where E_{initial} is the starting potential and v is the scan rate.

Thus, under conditions where this relationship holds, and a waveform where $\Delta E_i \propto 1/\sqrt{\omega_i}$ is applied in a single experiment the fundamental harmonic peak current is such that $I_p(\omega t) \propto \omega^{\frac{1}{2}}\Delta E$. Reversibility, achieved when $k^{o'}$ is very large, is rapidly recognised when using the custom-designed waveform by detection of a fundamental harmonic peak height ($I_p(\omega t)$) that is independent of frequency. In the case of quasi-reversibility, a characteristic frequency dependence is also detected in which $I_p(\omega t)$ decreases with increasing frequency, as also occurs if uncompensated resistance is significant. Finally, it is noted that traditionally when waveforms with constant ΔE values are used, the background current, which is proportional to ω, becomes very large at high frequencies, making the faradaic current hard to detect. In the present case, the background current does not increase very dramatically with frequency and hence correction,

even at high frequencies, is facilitated.

2 Experimental

2.1 Instrumentation

Details of the FT-ac voltammetric instrumentation are provided in [13]. Initial estimates of the uncompensated resistance (R_u) values were obtained using a BAS (Bioanalytical Systems)-Epsilon potentiostat and applying a small potential step in a potential region where no faradaic current flows. Analysis of the charging current versus time curve allows R_u to be extracted, as described in reference [6].

2.1.1 Chemicals and reagents

All chemicals and the solvent dichloromethane were of reagent grade purity and used as received from the manufacturer (Aldrich). The deionized water was obtained from a MilliQ-MilliRho purification system.

2.1.2 Instrumentation and procedures

A conventional single compartment, three-electrode cell was employed in all voltammetric measurements, with glassy-carbon (GC, 7.07 mm^2), platinum (Pt, 3.14 mm^2) or gold (Au, 3.14 mm^2) macrodisk working electrodes, an Ag | AgCl (0.5 M KCl) reference electrode and a platinum wire auxiliary electrode. The disc-shaped working electrodes were constructed by sealing glassy-carbon or metal rods into insulating Kel-F sheaths with epoxy resin. Before use, the surfaces of these electrodes were manually polished with an aqueous slurry of 0.1 or 0.05 μm alumina particles (Bioanalytical Systems) on a Microcloth polishing cloth (Buehler, Lake Bluff, IL) and then rinsed thoroughly with water.

In initial experiments, GC, Au or Pt electrodes were immersed in 10 ml of aqueous solutions containing 0.100 mM; 0.202 mM; 0.300 mM; 0.404 mM; 1.00 mM or 2.00 mM Ferrocenemethanol (FcMeOH) with 0.50 M KCl as the supporting electrolyte. The oxidation of FcMeOH was used as an example of a reversible process. Other systems studied were: reduction of $[Ru(NH_3)_6]^{3+}$ (reversible)

and $[Fe(CN)_6]^{3-}$ (quasi-reversible), again in 0.50 M KCl aqueous electrolyte; and oxidation of FcMeOH (reversible) in dichloromethane (0.1 M Bu_4NPF_6). The latter was used to assess the impact of a high level of uncompensated resistance. Solutions were purged with nitrogen for at least 5 minutes prior to commencement of a voltammetric experiment. All experiments were carried out at (20±1)°C.

The waveform used in the FT-ac voltammetric experiments was a composite, eight component sine-wave signal superimposed onto the dc potential to give a total potential E_t where

$$E_t = E_{\mathrm{dc}} + \sum_{i=1}^{8} \Delta E_i \sin(\omega_i t), \tag{3}$$

with the frequencies, ω_i, and amplitudes, ΔE_i, as given in Table 1. The individual sine waves were not phase randomised, as is sometimes the case in experiments where all amplitudes are the same [11]. However, consideration was given to minimisation of overlap of higher harmonic terms on the basis of an algorithm available in the literature [11]. Instrumental and FT requirements mean that 2^n data points need to be obtained. The chosen scan rate and potential range specified in Table 1 meant that the combination given there was identified as being suitable for implementation of the designer waveform with minimal overlap from higher harmonic and frequency sum and difference terms. In particular, these nonlinear terms were not within 5–10 Hz of the 8 applied frequencies. The amplitudes were chosen to be in the range of 20 to 2 mV and the frequencies ranging from 34.94 to 1970.01 Hz are geometrically spaced over a range that allows a substantial faradaic component to be measured relative to background current, under all conditions. However, it may be noted that the number of sine waves chosen in the designer waveform need not be 8, nor have the specific frequencies selected for the present study.

2.1.3 Data analysis and simulations

The experimental data, obtained with the FT-ac instrumentation, yield current, time, and applied dc potential as the output information. The data are plotted as current versus time and then transformed into frequency-related power

spectra for further analysis.

The raw FT-ac data obtained from experiments contains a very large number of data points (2^{18}). Consequently, processing the full set of data is slow. For this reason, a 'decimation' data reduction process is implemented in the frequency domain, where the first 2^{15} data points present in the raw data are retained and all the higher frequency data is discarded before the inverse Fourier transform operation is applied. This strategy removes data that contains no information relevant to the electrochemical reaction ($> 2,000$ Hz) being studied, and significantly reduces the data file size needed for the iFT operation while maintaining all useful information.

Another problem with raw ac data is the presence of background (charging) current. It is well known that in the fundamental harmonic response, the background current may dominate the voltammetry, particularly at high frequency, so that quantitative analysis of the faradaic component associated with electron transfer may require employment of a background correction procedure. Measurement of the background current at selected potential ranges on both sides of the region where Faradaic current is detected, interpolation to give values in this potential region using a polynomial fit and vectorial subtraction of the calculated background were used in the present case. The background current does not contribute significantly to the second and higher harmonic ac voltammograms. Consequently, background correction is unnecessary for measurement of these higher order components.

Analysis of the kinetics was based on peak height versus frequency profiles. However, full simulations were carried out using the procedure described below. Fitting of experimental data with simulated results for the quasi-reversible process was undertaken in an essentially heuristic manner:

Step 1. Identify the reversibility or otherwise of an electrode process by examining the lowest concentration data set, where the IR_u influence should be minimal, and compare it against predictions based on the reversible case (i.e. $I_p(\omega t)$ is constant for all 8 sine waves). If $I_p(\omega t)$ is independent of frequency, then the system under study is concluded to be reversible.

Step 2. Analyse data at higher concentrations and check if $I_p(\omega t)$ versus fre-

quency profiles are independent of concentration. If concentration dependence is detected, check if it is consistent with the increasing importance of the IR_u drop.

Step 3. To determine the contribution from the IR_u drop or quasi-reversibility, make initial estimates of values for parameters needed in numerical simulation. For instance, make an initial estimate of the value of $E^{o'}$, using $E^{o'} = (E_p^{\text{ox}} + E_p^{\text{red}})/2$, where E_p^{ox} and E_p^{red} are the peak potentials for the oxidation and reduction currents, respectively, in the aperiodic dc component. R_u can be evaluated immediately, as described in reference [6], and C_{dl} can be estimated from the magnitude of the fundamental harmonic current. In this study, initial guesses of diffusion coefficient values (D) are taken from the literature [6, 14–16] and are 7.6×10^{-6} cm^2 s^{-1} for FcMeOH, 8.0×10^{-6} cm^2 s^{-1} for $[Ru(NH_3)_6]^{3+}$ and 6.3×10^{-6} cm^2 s^{-1} for $[Fe(CN)_4]^{3-}$. In practice it was found that a value of $7.6 \pm 0.5 \times 10^{-6}$ cm^2 s^{-1} could be used for all three species in 0.50 M KCl under conditions of the present study.

Step 4. Compare simulations against experimental results until the level of desired accuracy is reached. Estimates of $E^{o'}$, D and R_u (k_0 and α if required) may need to be refined by comparing simulated and experimental peak currents, and wave shapes.

2.2 Simulations

We consider only the case of a macro-disk electrode: in doing so, we follow previous work [2, 8, 9] and invoke the assumption that diffusion is a one dimensional process.

2.2.1 Modelling the reaction mechanism

The system considered is one of semi-infinite mass transport to a planar electrode where a simple reduction or oxidation reaction occurs. This type of reac-

tion is commonly referred to as an E process and is represented as follows,

$$A + ne^- \underset{k_b}{\overset{k_f}{\rightleftharpoons}} B, \tag{4}$$

where both A and B are soluble in the solution phase; k_f and k_b are the forward and backward potential-dependent rate constants associated with Butler-Volmer kinetics [17], given by

$$k_f = k_0^{'} \exp\left(-\frac{\alpha n F}{RT}[E(t) - E^{o'} - I(t)R_u]\right), \tag{5}$$

$$k_b = k_0^{'} \exp\left((1-\alpha)\frac{nF}{RT}[E(t) - E^{o'} - I(t)R_u]\right), \tag{6}$$

with $E(t)$ being the applied potential (the exact form of which is described in the next paragraph), R_u is the uncompensated resistance, $I(t)$ is the total current and all other symbols as defined previously or as conventionally used.

The number of electrons transferred in the reaction, n, may be assigned as positive or negative so that both oxidation and reduction reactions are covered by the treatment that follows. By convention, our voltammetric experiments will begin at time $t = 0$: at time $t < 0$ the electrode is held at a constant initial potential, E_i, which is sufficiently extreme to ensure that the reaction in Equation (4) does not occur significantly. For $t > 0$, the time-dependent applied potential $E(t)$ has two components, a dc ramp denoted by $E_{\rm dc}$, and an oscillatory component which constitutes the 'designer' waveform represented by $E_{\rm ac} = \sum_{i=1}^{8} \Delta E_i \sin(\omega_i t)$, where ΔE_i are the amplitudes corresponding to each of the frequencies, ω_i, respectively, and these obey the following relation $\Delta E_i = \Delta E_1/\sqrt{\omega_i/\omega_1}$, where ΔE_1 is the amplitude of the first sine wave and ω_1 is the corresponding frequency. Note that we are using eight sine waves to mimic what has been done in the experiments. However, the theory can be applied to as many sine waves as may be desired by the user. Therefore the potential is given by the relationship

$$E(t) = E_{\rm dc}(t) + E_{\rm ac}(t), \tag{7}$$

$$= E_{\rm i} + vt + \sum_{i=1}^{8} \Delta E_i \sin(\omega_i t), \tag{8}$$

where v is the scan rate and has the same sign as n and $E_{\rm i}$ is the initial dc

potential. Also we have that

$$I(t) = I_f(t) + I_c(t), \tag{9}$$

$$\text{where} \quad I_c = C_{\text{dl}} \frac{\mathrm{d}E}{\mathrm{d}t}, \tag{10}$$

I_c is referred to as the capacitive current and I_f is the faradaic current (see definition in Section 2.2.2).

Mass transport to the electrode is then modelled by a linear diffusion equation for each species (A, B). If we let $c_{\text{A}}(x,t)$ and $c_{\text{B}}(x,t)$ represent the concentrations of species A and B, respectively, and let x represent the distance from the electrode surface at time t, we get the following system of equations,

$$\frac{\partial c_{\text{A}}}{\partial t} = D_{\text{A}} \frac{\partial^2 c_{\text{A}}}{\partial x^2}, \tag{11}$$

$$\frac{\partial c_{\text{B}}}{\partial t} = D_{\text{B}} \frac{\partial^2 c_{\text{B}}}{\partial x^2}, \tag{12}$$

where D_{A} and D_{B} are the diffusion coefficients for each of the species A and B, respectively.

In many studies, microelectrodes (radial diffusion dominant) are used instead of macroelectrodes (linear diffusion dominant) in order to minimise the IR_u drop and the charging current. We have previously studied the effects of the use of microelectrodes in ac voltammetry [7] and have derived precise conditions under which the effects of radial diffusion can be neglected. This work demonstrates, both theoretically and experimentally, that the effects of radial diffusion are much lower in the ac voltammetry case and these results carry through directly tot he designer waveform introduced in this paper.

2.2.2 Boundary conditions

Given that we have made the assumption of semi-infinite linear diffusion, we have the following boundary and initial conditions:

$$\text{at } x = 0 \quad D_{\text{A}} \frac{\partial c_{\text{A}}}{\partial x} = -D_{\text{B}} \frac{\partial c_{\text{B}}}{\partial x} = \frac{I_f(t)}{nAF} = k_f c_A - k_b c_B; \tag{13}$$

$$\text{as } x \to \infty \quad c_{\text{A}} = c_{\text{A}}^*, \quad c_{\text{B}} = 0; \tag{14}$$

$$\text{and at } t = 0 \quad c_{\text{A}} = c_{\text{A}}^*, \quad c_{\text{B}} = 0. \tag{15}$$

Here, c_{A}^{*} is the bulk concentration of species A and $I_f(t)$ is the faradaic current. Note that the equation involving $I_f(t)$ in Equation (13) is derived from Fick's first and Faraday's laws.

2.2.3 Non-dimensional variables

As has been discussed elsewhere [8, 18], we re-cast the problem in terms of non-dimensional variables: these dimensionless variables will be assigned Greek symbols in order to improve clarity. The nature of the problem implies a linear relationship between time t and the dc component of applied potential, E_{dc}, therefore the dimensionless symbol τ can be defined by

$$\tau = F(E_{\mathrm{init}} + vt - E^{o'})/RT = F(E_{\mathrm{dc}} - E^{o'})/RT, \tag{16}$$

and is used to replace both of these dimensional variables.

The sine wave amplitudes ΔE_i are similarly non-dimensionalised to obtain

$$\Delta\tau_i = \frac{F\Delta E_i}{RT}, \tag{17}$$

whilst the angular frequency ω_i becomes

$$\Omega_i = \frac{RT\omega_i}{Fv}. \tag{18}$$

This now allows us to write down a non-dimensional version of Equation (8), using Equations (16)-(18), where $\epsilon(\tau)$ is the non-dimensional potential

$$\epsilon(\tau) = \epsilon_{\mathrm{dc}}(\tau) + \epsilon_{\mathrm{ac}}(t), \tag{19}$$

$$= \tau + \sum_{i=1}^{8} \Delta\tau_i \sin(\Omega_i \tau). \tag{20}$$

Note that R_u and $I_{\mathrm{tot}}(t)$ are nondimensionalised as follows

$$\rho_u = \frac{F^2 A D_A c_A^*}{RT}\left(\frac{vF}{D_A RT}\right)^{\frac{1}{2}} R_u, \tag{21}$$

$$\iota_{\mathrm{tot}}(\tau) = \left(\frac{D_A RT}{vF}\right)^{\frac{1}{2}} \frac{I_{\mathrm{tot}}(t)}{AFD_A c_A^*}; \tag{22}$$

faradaic and capacitive currents are non-dimensionalised in the same way as for the total current, $I_{\mathrm{tot}}(t)$. Finally the double layer capacitance constant is non-dimensionalised as follows

$$\gamma_{\mathrm{dl}} = \left(\frac{D_A RT}{Fv}\right)^{\frac{1}{2}} \frac{vC_{\mathrm{dl}}}{AFD_A c_A^*}. \tag{23}$$

2.2.4 Numerical methods

The numerical algorithm used to solve the equations in Section 2.2.1 involves backward Euler discretisations [19], along with a simple expanding mesh in space, as described in [2]. We also make use of Brent's method to deal with the nonlinearity introduced via the inclusion of uncompensated resistance and double layer capacitance [20].

Data analysis of simulation results is carried out in the frequency domain using Fourier analysis (via FFTs). This allows us to pick out the dc component of the signal as well as the harmonics of interest in a straightforward manner, again as described previously in [2]. The 'decimation' process is done in the frequency domain, where the first 2^n data points are retained and the data at higher frequencies is discarded before the inverse Fourier transform is applied.

3 Results and discussion

3.1 Experimental aspects of multi-frequency and variable amplitude ac voltammetry for a reversible process

Figure 1 illustrates the steps required for analysis of an electrode process after collection of data in the *I-t* format, using the multi-frequency and variable-amplitude designer waveform FT-ac voltammetry. The example presented is for the oxidation of moderately low 0.404 mM concentration of FcMeOH in aqueous 0.5 M KCl electrolyte at a GC electrode. According to literature reports [6]. FcMeOH is oxidised reversibly to $[\mathrm{FcMeOH}]^+$ by a simple, outer-sphere, one-electron charge transfer process

$$\mathrm{FcMeOH} \rightleftharpoons [\mathrm{FcMeOH}]^+ + e^-. \tag{24}$$

Figure 1(a) demonstrates clearly that this new designer form of FT-ac voltammetry generates a vast amount of data which can be displayed in the *I-t* format (Figures 1(a) and (b))), or as the power spectrum (Figure 1(c)) in the frequency domain. The power spectrum provides a convenient overview of the relative significance of dc and ac terms. The 'noisy' nature of the power spectrum (Figure 1(c)) implies, as expected, that this new form of ac voltammetry contains a very large amount of ac harmonic information. The dc aperiodic component (Figure 1(d)), the fundamental (Figure 1(e)–(g)), higher ac harmonics (Figure 1(h)–(n)) and frequency sum and difference terms (not shown), are derived by use of the power spectrum and the inverse FT algorithm. For the medium to fairly small amplitude case used in experimental studies, the second ac harmonic component (Figure 1(j)) may be identified at all frequencies, although the third harmonic (Figure 1(m)) can become obscured by the system noise. In the highest frequency, minimum ΔE, case, where $\Delta E = 2.66$ mV, the contribution from nonlinearity is minimal.

In order to display the harmonic information in a clearer form, the eight fundamental harmonics can be presented in raw (Figures 2(a) and (b)), decimated (Figures 2(c) and (d)) and background corrected (Figures 2(e) and (f)) format,

which readily reveals the peak current $I_p(\omega t)$, values associated with each of the eight frequencies in the designer waveform.

Figure 2(d) depicts the fundamental harmonic response for the 8 frequencies in ac *I-t* format after applying the 'decimation' process. The result is indistinguishable from that produced by analysis of the full data set (Figure 2(b)).

A significant frequency-dependent background charging current contribution is clearly observable in the fundamental ac harmonics (Figure 2(b)). The background current corrected results in Figure 2(f) reveal that the peak heights associated with the Faradaic process are independent of frequency, within experimental error, as predicted theoretically for a reversible process.

3.2 Simulation of the FT-ac voltammetry

Simulations of the fundamental harmonic ac voltammetry obtained for a reversible process ($k_0^{'} = 10,000$ cm s^{-1} and $\alpha = 0.5$) with the designer waveform and parameters given in Table 1 along with: $R_u = 0$ Ω; $C_{\rm dl} = 0.09$ Fm^{-2}; $E^{o'} = 0.185$ V; and $D = 7.6 \times 10^{-6}$ cm^2 s^{-1} (Figure S-1(a) and (b)), are in excellent agreement with experimental data (provided in Figure 2(a) and (b)).

If zero capacitance is employed instead of 0.09 F m^{-2} in the simulation, as is the case in Figure S-2, then excellent agreement is achieved with background current corrected experimental data given in Figure 2(e) and (f). This result demonstrates the effectiveness of background current correction software used in this study.

3.3 Application of the designer waveform to the [FcMeOH]$^{0/+}$ process as a function of concentration

Ideally, the reversible [FcMeOH]$^{0/+}$ process should exhibit $I_p(\omega t)$ values that are independent of frequency for all concentrations, when using the designer waveform. This is true for FcMeOH concentrations ≤ 0.404 mM (see Figure S-2 for 0.404 mM case). However, less conformity to this predicted response was obtained at higher FcMeOH concentrations. In particular, significant de-

viation from $I_p(\omega t)$ being independent of frequency was obtained (Figure 3) with a 2.00 mM FcMeOH solution, even though the background correction is relatively unimportant for this data set. Data obtained at $\geq$ 1 mM FCMeOH concentration resemble that expected for a quasi-reversible process.

The major factor contributing to the apparently non-reversible behaviour at higher FcMeOH concentrations is the presence of an uncompensated (Ohmic) IR_u drop which becomes more important as the concentration (current) is increased. The IR_u drop can lead to significant distortion in FT-ac voltammetry [13]. The predicted effect on designer-waveform FT-ac voltammetry is illustrated by simulations shown in Figure 4, with $R_u = 100\ \Omega$. In the present experiment at a GC electrode with 0.50 M KCl as the electrolyte, R_u is experimentally estimated to be 20 Ω. Simulations confirm that this value is not expected to be important at low concentrations of FcMeOH but, as found experimentally, does have an impact upon data of concentrations $\geq$ 1 mM.

For the theory of the designer waveform to be fully valid, surface interactions between FcMeOH (or $[FcMeOH]^+$) and the electrode should be absent. A useful method of checking for surface interaction is to compare the background current in 0.50 M KCl before and after addition of FcMeOH. As shown in Figure S-3, the background current at the glassy carbon electrode is reduced by a small amount after addition of 2.0 mM FcMeOH to 0.50 M KCl electrolyte. No differences in background current were detected on addition of FcMeOH concentrations $\leq$ 0.404 mM. The implication of this result is that FcMeOH (and $[FcMeOH]^+$) adsorbs weakly onto a glassy carbon electrode, resulting in a small reduction in the double layer capacitance. In contrast the background current at platinum and gold electrodes in 0.50 M KCl is indistinguishable in the presence or absence of 2.0 mM FcMeOH, which indicates that FcMeOH does not adsorb at a detectable level at these electrode surfaces. Additionally, R_u is only 10 Ω at these electrode surfaces compared to 20 Ω at the GC electrode so that $I_p(\omega t)$ values at platinum or gold electrodes, even with 2.0 mM FcMeOH present, are closer to a constant than at the GC surface. Clearly, taking R_u and surface interactions into account may be necessary if the use of the designer-waveform to detect reversibility is to be correctly implemented.

Clearly, background current correction becomes highly critical, particularly at high frequencies and low concentrations of FcMeOH, where the background current may produce a significant component of the total current. Figure S-4 illustrates the FT-ac voltammetry at a GC electrode in 0.50 M KCl electrolyte with 0.100 mM FcMeOH.

The instrumental background current correction implemented in this work uses baseline-subtraction software in a user-interactive mode. Thus, data are chosen at user-selected times at either side of the $[FcMeOH]^{0/+}$ or other process. A polynomial fit to both data sets and interpolation to potentials in between, leads to a predicted background at potentials where a Faradaic current is present. Obviously, there is a small level of uncertainty in this approach. Figure S-4 contains the background corrected faradaic current, for a dilute 0.100 mM FcMeOH solution using the polynomial fit derived from either 0.5–1.5 and 11–12 s, or 0–1 and 10–11 s zones for the correction of the raw data. Even with this more severe background problem than used in studies at higher concentration referred to above, excellent correction is still achieved. Traditionally, all sine waves used in multi-waveform approaches use constant values of ΔE and so the background current increases with frequency. The designer-waveform mitigates problems with large background current at higher frequencies.

An alternative means of background current correction is to undertake measurements in the base electrolyte to produce the 'blank background current file'. When 0.50 M KCl was used to produce the 'blank background current file' for correction of experimental data, this form of correction worked well at gold and platinum electrodes. However, it should be noted that this 'blank background current file' correction method is applicable only if adsorption is negligible, which is not perfectly true when high concentrations of FcMeOH are oxidised at a GC electrode. In general, the instrumental method is rapid and reliable, provided the zones used for background fitting are selected sensibly. This method is therefore recommended as a generally applicable and convenient approach for dealing with the background current correction.

3.4 Comparison of the designer waveform with other FT–ac methods

An alternative approach to the use of the designer waveform introduced in this study is to use eight sine waves individually in eight experiments instead of simultaneously in just one experiment. $I_p(\omega t)$ values using this single sine wave version are similar (Figure 5). However, the ability to obtain all data from a single experiment is clearly a significant advantage of the far more efficient designer waveform. Alternatively, one can employ the same frequency set as in Table 1 but with a constant amplitude for all frequencies. Data obtained from this more conventional experiment with $\Delta E = 15$ mV for all frequencies are shown in Figure 6. As expected, the values of $I_p(\omega t)$ now increase with frequency. However, the IR_u drop now becomes even more significant at higher frequencies, as does the background current.

Another alternative is to use a square-wave FT-ac method [9, 21–23] which utilises a variable amplitude waveform at frequencies ωt, $3\omega t$, $5\omega t$ etc. A square-wave experiment is equivalent to applying $k = (K + 1)/2$ sine waves of varying amplitude where K is an odd natural number [23]. In this case, the square-wave can be written as

$$E_{\text{square-wave}} = \sum_{m=1,3}^{k} \frac{4\Delta E}{m\pi} \sin(m\omega t), \tag{25}$$

and the amplitude $(4\Delta E/m\pi)$ of each component $(m\omega t)$ clearly becomes smaller as m increases.

Figure 6 provides a comparison of $I_p(\omega t)$ values obtained from the designer waveform, the conventional constant amplitude sinusoidal waveform and the square wave methods of FT-ac voltammetry for oxidation of 0.404 mM FcMeOH at a GC electrode, as a function of frequency. Only $I_p(\omega t)$ values obtained from the designer waveform are independent of frequency for a reversible process, allowing ready assignment of very fast electrode kinetics. $I_p(\omega t)$ values obtained from the square-wave decrease with frequency as expected, while from a multi-frequency, fixed 15 mV amplitude voltammetric experiment, $I_p(\omega t)$ increases with frequency, also as expected (approximately square root dependency).

3.5 Application of the designer waveform to other processes

A more limited set of experiments were also undertaken with the designer waveform on the reduction of 0.300 mM $[Ru(NH_3)_6]^{3+}$ and 0.300 mM $[Fe(CN)_6]^{3-}$ in aqueous 0.50 M KCl electrolyte. As for oxidation (the $[FcMeOH]^{0/+}$ process), the one-electron reduction of $[Ru(NH_3)_6]^{3+}$ to $[Ru(NH_3)_6]^{2+}$ is believed to involve a fast outer-sphere reversible electron-transfer process [4, 16]. For this process, $I_p(\omega t)$ values of background-corrected fundamental harmonic currents are close to constant at GC, platinum and gold electrodes. In this case, essentially identical background currents were obtained before and after $[Ru(NH_3)_6]^{3+}$ addition to 0.50 M KCl, implying that, adsorption is absent at all three electrode surfaces. Simulations based on a reversible process confirm that the reaction can be regarded as being very close to reversible with frequencies up to almost 2 kHz ($k^0 \geq 1$ cm s^{-1}).

A very different dependence of $I_p(\omega t)$ on frequency is found for the reduction of $[Fe(CN)_6]^{3-}$ at a GC electrode in aqueous 0.50 M KCl electrolyte (Figure 7). Data obtained at Pt or Au electrodes have quasi-reversible characteristics similar to those at GC electrodes. Comparison of background currents before and after the addition of $[Fe(CN)_6]^{3-}$ to 0.50 M KCl electrolyte suggest adsorption is minimal at all three electrode surfaces.

Simulations of a quasi-reversible process using $D = 7.6 \times 10^{-6}$ cm^2 s^{-1}; $R_u = 0$ Ω, $C_{\rm dl} = 0.15$ Fm^{-2}; $E^{o'} = 0.278$ V, $k_0^{'} = 0.023$ cm s^{-1} and $\alpha = 0.5$, provided an excellent fit to experimental $I_p(\omega t)$ values (Figure 8). Clearly, the designer waveform can be used to show departure from reversibility and then to estimate kinetic parameters for a quasi-reversible electrochemical system.

Experiments have also been carried out with the designer waveform for oxidation of FcMeOH at a glassy carbon electrode in the very high resistance dichloromethane (0.10 M Bu_4NPF_6) medium. The FT-ac data obtained are shown in Figure 9(a). Simulations using parameters $R_u = 1100$ Ω, $C_{\rm dl} = 0.13$ Fm^{-2}, $E^{o'} = -0.154$ V, with reversible electrode kinetics ($k_0^{'} = 10,000$ cm s^{-1}; and $\alpha = 0.5$) agree well with experimental data. Although the resistance of

this medium is high, the oxidation of FcMeOH is shown to remain reversible, as found in aqueous media. However, in this case, $I_p(\omega t)$ is not independent of frequency because of the significant contribution of the IR_u drop. In this case, direct proof of reversibility is not possible via casual inspection the plot of $I_p(\omega t)$ versus frequency. However, before assuming a process is quasi-reversible rather than reversible, studies on the concentration dependence and simulations that take R_u into account must be employed.

4 Conclusions

A multi-frequency, variable amplitude 'designer waveform' consisting of eight sine waves of amplitude from 20 mV to about 2 mV with frequencies covering the range 35 to 1970 Hz has been developed to facilitate rapid assessment of the reversibility or otherwise of electrode processes by FT-ac voltammetry. With this waveform, $I_p(\omega t)$ for the fundamental harmonic of a reversible process is predicted to be independent of frequency, provided the influence of the IR_u drop is insignificant. Reversible oxidation of ferrocenemethanol (FcMeOH), reversible reduction of hexaminеruthenium ($[Ru(NH_3)_6]^{3+}$) and the quasi-reversible reduction of ferricyanide ($[Fe(CN)_6]^{3-}$) in aqueous 0.50 M KCl electrolyte have been studied at glassy carbon, gold and platinum electrodes in order to assess the attributes of the new waveform. A major advantage of the method was found to be ready access to efficient methods for obtaining and analysing large amounts of information generated from a single experiment. Analysis of both experimental and simulated data reveals the readily recognised patterns of behaviour that enable identification of reversibility or quasi-reversibility, and contributions from uncompensated resistance and background capacitance. Excellent agreement between experimental and simulated ac voltammograms was obtained for all processes examined in aqueous 0.50 M KCl electrolyte. Provided attention is paid to the IR_u drop, the waveform can also be used to confirm that oxidation of FcMeOH is reversible in highly resistive dichloromethane solvent.

5 Acknowledgements

Financial support from the Australian Research Council is gratefully acknowledged.

6 Supplementary Material

Figures S-1 to S-4 contain ac voltammetric data. Supplementary material associated with this article can be found, in the online version, at doi:XXX

References

[1] S. O. Engblom, J. C. Myland, and K. B. Oldham. Must ac voltammetry employ small signals? *J. Electroanal. Chem.*, 480:120, 2000.

[2] D. J. Gavaghan and A. M. Bond. A complete numerical simulation of the techniques of alternating current linear sweep and cyclic voltammetry: analysis of a reversible process by conventional and fast Fourier transform methods. *J. Electroanal. Chem.*, 480:133, 2000.

[3] D. E. Smith. *Electroanalytical Chemistry: A Series of Advances*, volume 1. Marcal Dekker, New York, 1966.

[4] J. Zhang, S. Guo, and A. M. Bond. Large amplitude Fourier transformed high-harmonic alternating current cyclic voltammetry: kinetic discrimination of interferring faradaic processes at glassy carbon and at boron doped diamond electrodes. *Anal. Chem.*, 76:3619, 2004.

[5] S. Guo, J. Zhang, D. Elton, and A. M. Bond. Fourier transform large-amplitude alternating current cyclic voltammetry of surface-bound azurin. *Anal. Chem.*, 76:166, 2004.

[6] B. Lertanantawong, A. P. O'Mullane, J. Zhang, W. Surareungchai, M. Somasundrum, and A. M. Bond. Investigation of mediated oxidation of ascorbic acid by ferrocenemethanol using large-amplitude Fourier transformed ac voltammetry under quasi-reversible electron-transfer conditions at an indium tin oxide electrode. *Anal. Chem.*, 80:6515, 2008.

[7] D. J. Gavaghan, D. M. Elton, and A. M. Bond. Numerical simulation of alternating current linear sweep voltammetry at microdisc electrodes. *Collect. Czech. Chem. Commun.*, 66:255, 2001.

[8] D. J. Gavaghan, D. Elton, and A. M. Bond. A comparison of sinusoidal, square wave, sawtooth, and staircase forms of transient ramped voltammetry when a reversible process is analysed in the frequency domain. *J. Electroanal. Chem.*, 513:73, 2001.

[9] D. J. Gavaghan, D. Elton, K. B. Oldham, and A. M. Bond. Analysis of

ramped square-wave voltammetry in the frequency domain. *J. Electroanal. Chem.*, 512:1, 2001.

[10] M. Rosvall and M. Sharp. A complete system for electrochemical impedance spectroscopy which combines FFT methods and staircase voltammetry. *Electrochem. Commun.*, 2:338, 2000.

[11] J. Hàzí, D. M. Elton, W. A. Czerwinski, V. A. Vicente-Beckett, and A. M. Bond. Microcomputer-based instrumentation for multi-frequency Fourier transform alternating current (admittance and impedance) voltammetry. *J. Electroanal. Chem.*, 437:1, 1997.

[12] J. Schiewe, J. Hàzí, V. A. Vicente-Beckett, and A. M. Bond. A unified approach to trace analysis and evaluation of electrode kinetics with fast Fourier transform electrochemical instrumentation. *J. Electroanal. Chem.*, 451:129, 1998.

[13] A. M. Bond, N. W. Duffy, S. Guo, J. Zhang, and D. Elton. Changing the look of voltammetry. Can FT revolutionize voltammetric techniques as it did for NMR? *Anal. Chem.*, 77:186A, 2005.

[14] M. P. Longinotti and H. R. Corti. Diffusion of ferrocene methanol in supercooled aqueoue solutions using cylindrical microelectrodes. *Electrochem. Commun.*, 9:1444, 2007.

[15] C. Cannes, F. Kanoufi, and A. J. Bard. Cyclic voltammetry and scanning electrochemical microscopy of ferrocenemethanol at monolayer and bilayer-modified gold electrodes. *J. Electroanal. Chem.*, 547:83, 2003.

[16] M. Pyo and A. J. Bard. Scanning electrochemical microscopy. 35. Determination of diffusion coefficients and concentrations of $Ru(NH_3)_6^{3+}$ and methylene blue in polyacrylamide films by chronoamperometry at ultramicrodisk electrodes. *Electrochim. Acta*, 42:3077, 1997.

[17] A. J. Bard and L. R. Faulkner. *Electrochemical Methods*. Wiley, New York, 2nd edition, 2001.

[18] D. J. Gavaghan and A. M. Bond. Numerical simulation of the effects of

experimental error on the higher harmonic components of Fourier transformed ac voltammetry. *Electroanal*, 18:333, 2006.

[19] K. W. Morton and D. F. Mayers. *Numerical Solution of Partial Differential Equations*. Cambridge University Press, Cambridge, 1994.

[20] R. Brent. *Algorithms for Minimization without Derivatives*. Prentice Hall, England, 1973.

[21] A. A. Sher, A. M. Bond, D. J. Gavaghan, K. Harriman, S. W. Feldberg, and N. W. Duffy. Resistance, capacitance, and electrode kinetic effects in Fourier-transformed large-amplitude sinusoidal voltammetry: emergence of powerful and intuitively obvious tools for recognition of patterns of behaviour. *Anal. Chem.*, 76:6214, 2004.

[22] A. M. Bond. *Modern Polarographic Methods in Analytical Chemistry*. Marcal Dekker, New York, 1980.

[23] A. A. Sher, A. M. Bond, D. J. Gavaghan, K. Gillow, N. W. Duffy, S. Guo, and J. Zhang. Fourier transformed large amplitude square-wave voltammetry as an alternative to impedance spectroscopy: Evaluation of resistance, capacitance and electrode kinetic effects via an heuristic approach. *Electroanal.*, 17:1450, 2005.

Figure Legends

Figure 1. (a) Raw *I-t* data obtained at a GC electrode for oxidation of 0.404 mM FcMeOH in 0.5 M KCl. (b) 1:8 decimated data. (c) Power spectrum obtained after FT. (d)–(m) i-FT-recovered dc, 1st, 2nd and 3rd harmonic responses (only those derived from sine waves at 34.94 Hz, 370.00 Hz and 1970.01 Hz) are shown.

Figure 2. (a) Raw *I-t* data obtained at a GC electrode for oxidation of 0.404 mM FcMeOH in 0.5 M KCl. (b) FT-recovered 1st harmonic for all eight component frequencies. (c) 1:8 decimated data. (d) FT-recovered fundamental harmonics from 1:8 decimated ac voltammogram for all eight component frequencies. (e) Decimated and background current corrected data. (f) FT-recovered fundamental harmonic responses from 1:8 decimated data and background current corrected ac voltammogram for all frequencies.

Figure 3. Background corrected $I_p(\omega t)$ vs frequency data obtained from FT-ac voltammetry at a GC electrode for oxidation of designated FeMeOH concentrations in 0.50 M KCl.

Figure 4. (a) FT-recovered fundamental harmonic ac voltammograms simulated for a reversible process with, $R_u = 100\ \Omega$ and $C_{\rm dl} = 0\ {\rm Fm}^{-2}$. Other parameters used in simulation are as for Figure S-1. (b) Experimental and simulated data (0.50 M KCl with 0.404 mM FcMeOH) illustrating the influence of uncompensated resistance.

Figure 5. Comparison of I_p versus frequency data obtained from oxidation of 0.404 mM FcMeOH at a glassy carbon electrode in 0.50 M KCl using the designer variable amplitude waveform in one experiment versus using eight individual single-frequency measurements. Faradaic currents in both cases were corrected using the baseline-subtraction method.

Figure 6. $I_p(\omega t)$ values from oxidation of 0.4 mM FcMeOH in 0.50 M KCl at a glassy carbon electrode from FT-recovered fundamental harmonics as a function of frequency using the new designer waveform, fixed 15 mV

amplitude and square wave voltammetry.

Figure 7. (a) Raw I-t data obtained using the multi-time scale method for reduction of 0.300 mM $[Fe(CN)_6]^{3-}$ in 0.50 M KCl at a GC electrode. (b)-(i) FT-ac recovered fundamental harmonics for each frequency in I-t format. (j) FT-ac recovered 1st harmonics for all eight component frequencies in 'envelope' I_{amp}-t format.

Figure 8. (a) Simulated fundamental ac harmonics mimicking experimental data in Figure 7(j) in I_{amp} format. (b) Comparison of $I_p(\omega t)$ values obtained from experimental data and by simulation after background correction. Simulation parameters are provided in the text.

Figure 9. (a) Fundamental harmonic FT-ac voltammograms displayed in I_{amp}-t format for oxidation of 0.400 mM FeMeOH in dichloromethane (0.10 mM Bu_4NPF_6) at a GC electrode. (b) Simulated FT-ac voltammograms. (c) Comparison of experimental and simulated $I_p(\omega t)$ values before and after background correction.

Tables

Component	Frequency (Hz)	Amplitude (mV)
1	34.94	20.00
2	89.97	12.46
3	229.96	7.79
4	370.00	6.14
5	589.97	4.86
6	929.94	3.88
7	1369.98	3.19
8	1970.01	2.66

Table 1: Sine-wave components used in the composite designer waveform FT-ac voltammetric experiments. The dc potential range chosen for oxidation of FcMeOH in 0.50 M KCl is 0–500.00 mV vs. Ag | AgCl (selected 500 mV range chosen in other cases); the dc scan rate is 37.25 mVs^{-1}; the total number of data points collected is 2^{18}. Note that the choice of applied potential for each sine wave in this designer waveform is based on the relationship $\Delta E_i \propto \sqrt{\omega_i}$.

Figures

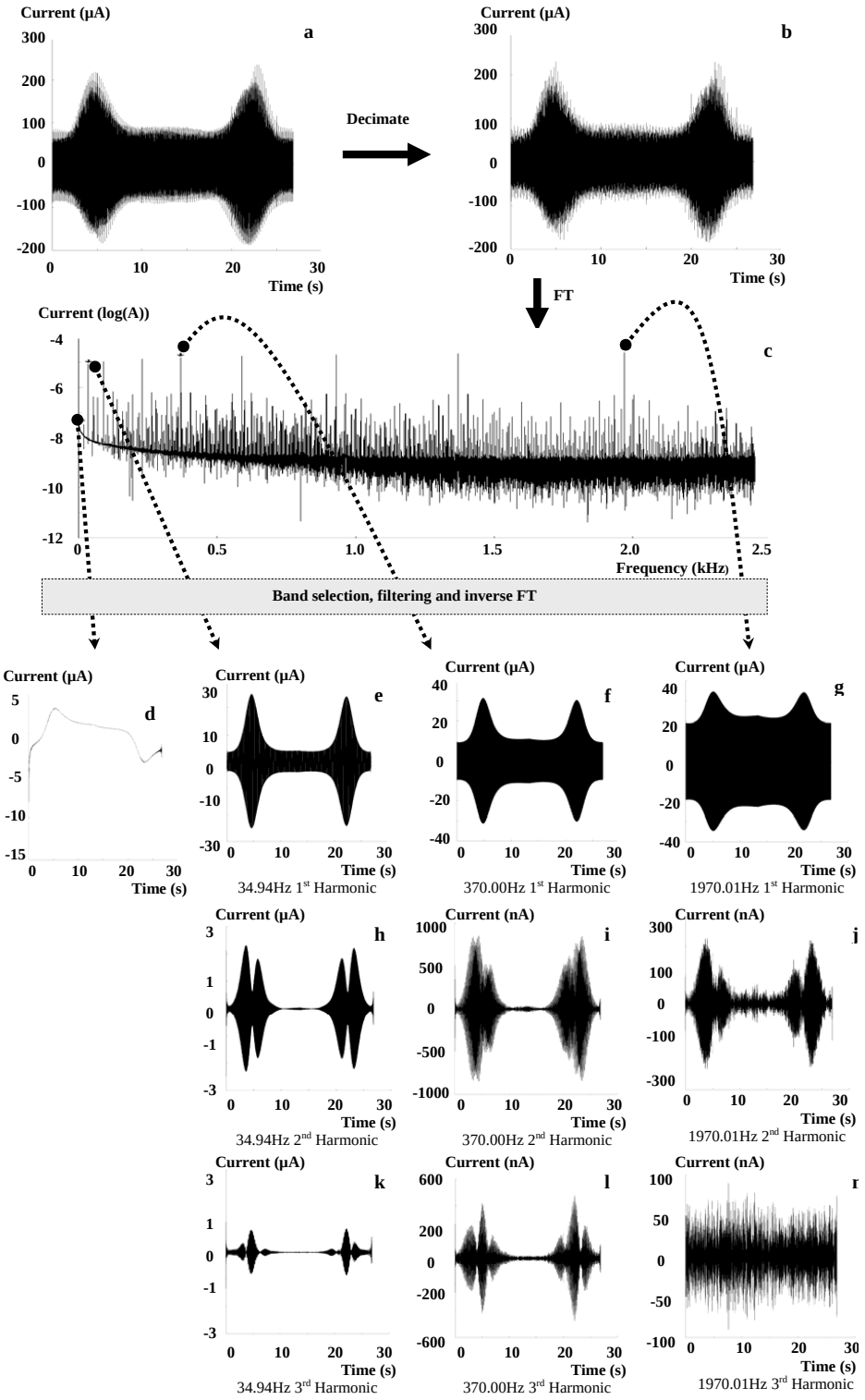
Current (µA)
a
Time (s)
Decimate
Current (µA)
b
Time (s)
FT
Current (log(A))
c
Frequency (kHz)
Band selection, filtering and inverse FT
Current (µA)
d
Time (s)
Current (µA)
e
Time (s)
34.94Hz 1st Harmonic
Current (µA)
f
Time (s)
370.00Hz 1st Harmonic
Current (µA)
g
Time (s)
1970.01Hz 1st Harmonic
Current (µA)
h
Time (s)
34.94Hz 2nd Harmonic
Current (nA)
i
Time (s)
370.00Hz 2nd Harmonic
Current (nA)
j
Time (s)
1970.01Hz 2nd Harmonic
Current (µA)
k
Time (s)
34.94Hz 3rd Harmonic
Current (nA)
l
Time (s)
370.00Hz 3rd Harmonic
Current (nA)
r
Time (s)
1970.01Hz 3rd Harmonic

Figure 1:

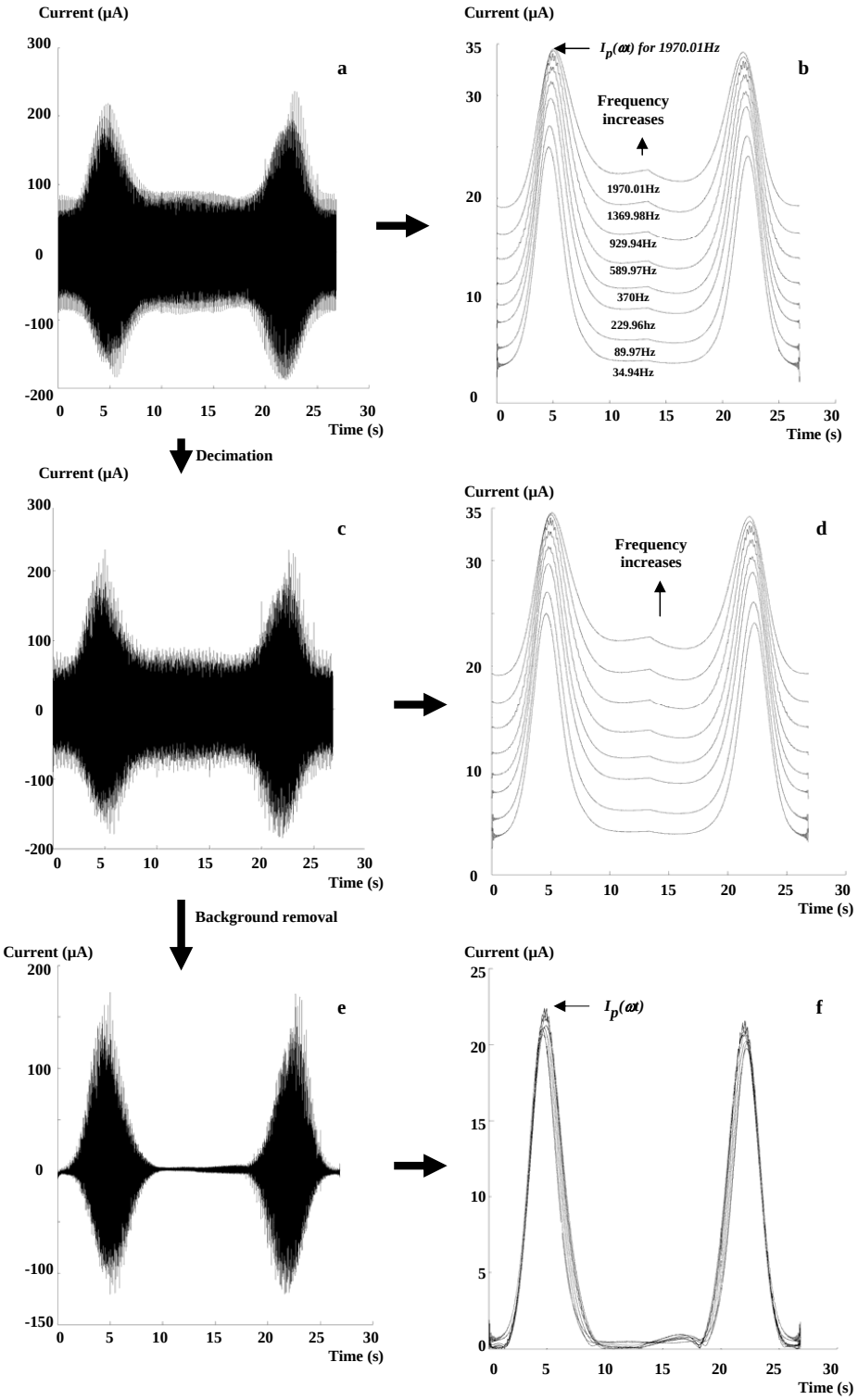
Current (μA)
a
Time (s)
Current (μA)
b
$I_p(\omega t)$ for 1970.01Hz
Frequency increases
1970.01Hz
1369.98Hz
929.94Hz
589.97Hz
370Hz
229.96hz
89.97Hz
34.94Hz
Time (s)
Decimation
Current (μA)
c
Time (s)
Current (μA)
d
Frequency increases
Time (s)
Background removal
Current (μA)
e
Time (s)
Current (μA)
f
$I_p(\omega t)$
Time (s)

Figure 2:

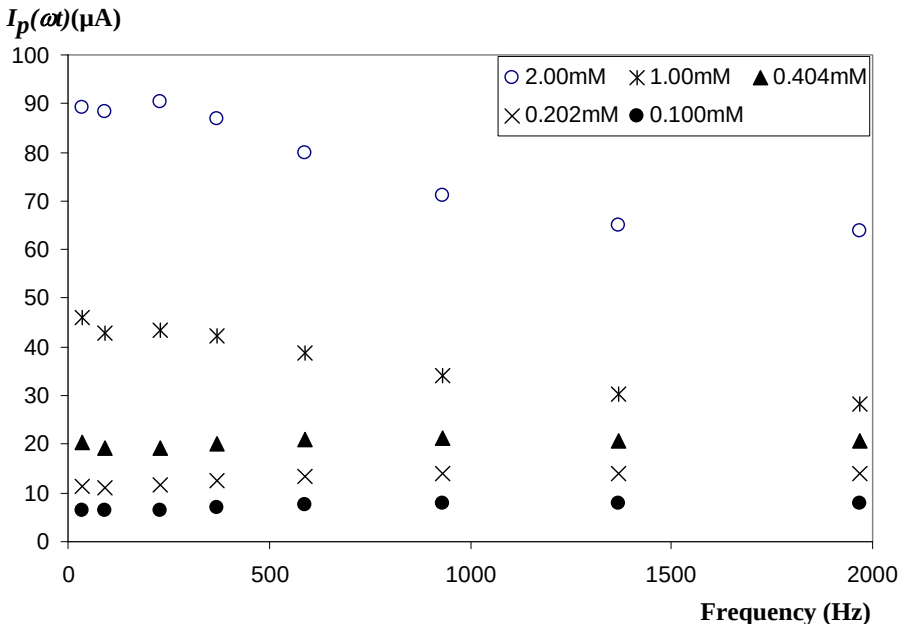
$I_p(\omega t)$(μA)
100
90
80
70
60
50
40
30
20
10
0
0
500
1000
1500
2000
Frequency (Hz)
2.00mM
1.00mM
0.404mM
0.202mM
0.100mM

Figure 3:

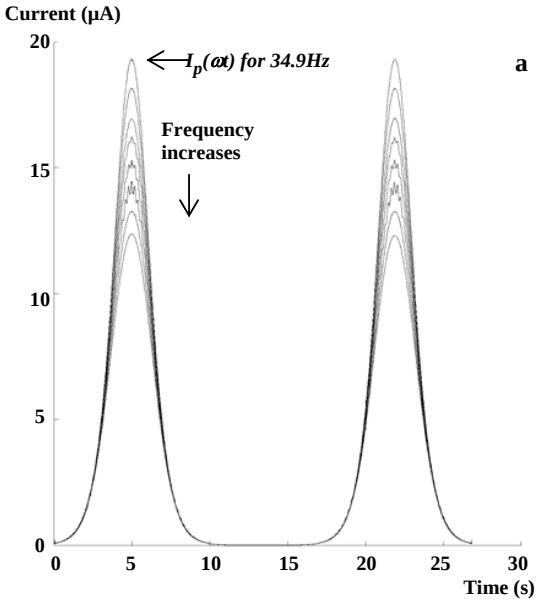
Current (μA)
20
15
10
5
0
$I_p(\omega t)$ for 34.9Hz
a
Frequency increases
0
5
10
15
20
25
30
Time (s)

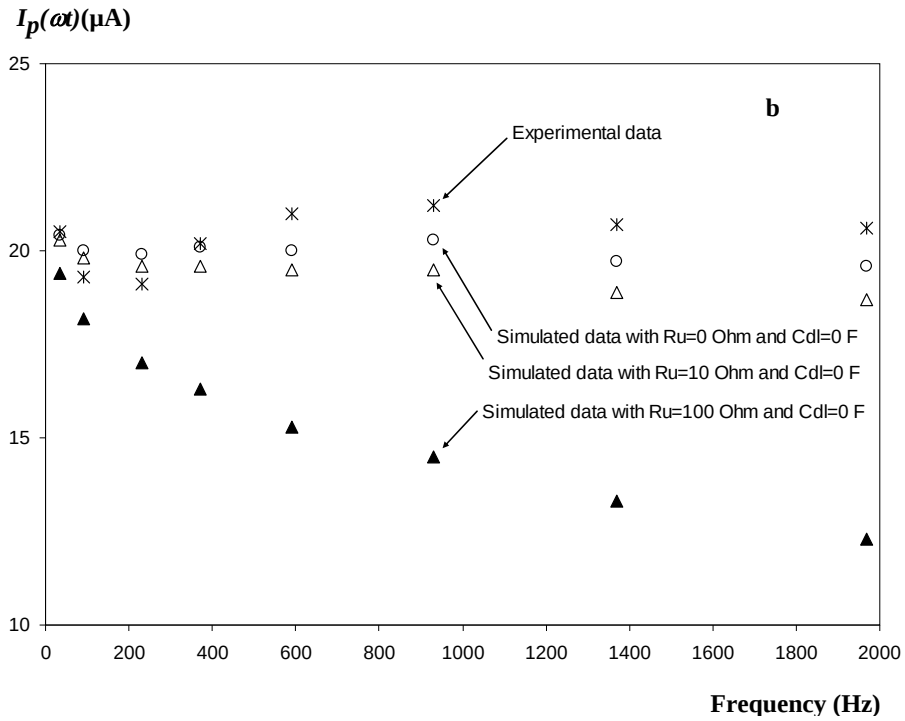
$I_p(\omega t)$(μA)
25
20
15
10
b
Experimental data
Simulated data with Ru=0 Ohm and Cdl=0 F
Simulated data with Ru=10 Ohm and Cdl=0 F
Simulated data with Ru=100 Ohm and Cdl=0 F
0
200
400
600
800
1000
1200
1400
1600
1800
2000
Frequency (Hz)

Figure 4:

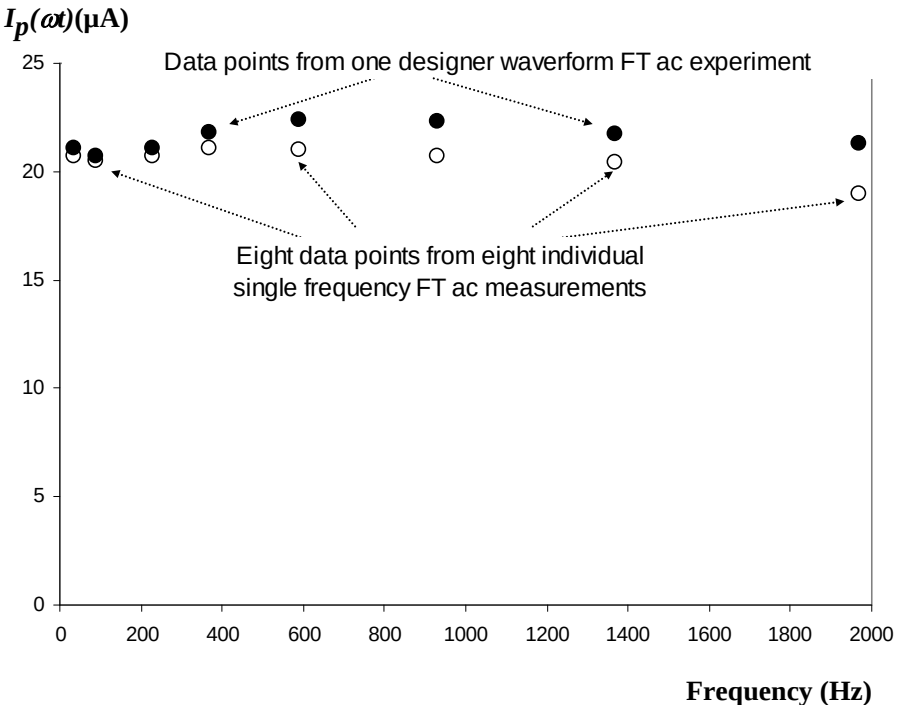
$I_p(\omega t)$(μA)
Data points from one designer waverform FT ac experiment
Eight data points from eight individual
single frequency FT ac measurements
25
20
15
10
5
0
0
200
400
600
800
1000
1200
1400
1600
1800
2000
Frequency (Hz)

Figure 5:

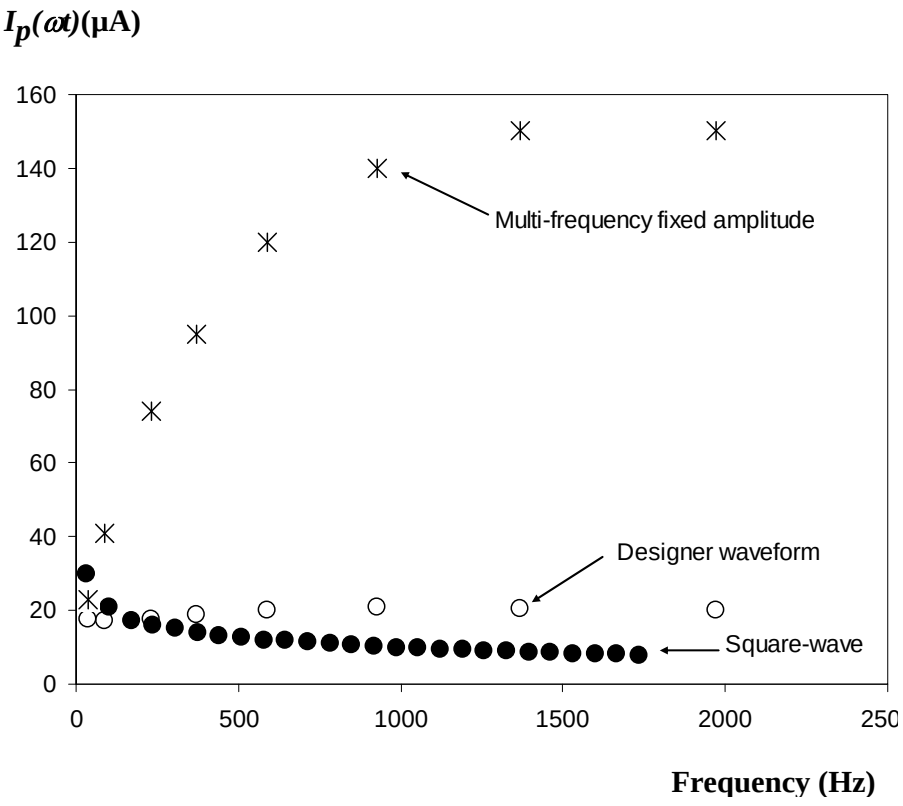
$I_p(\omega t)$(μA)
160
140
120
100
80
60
40
20
0
0
500
1000
1500
2000
250
Multi-frequency fixed amplitude
Designer waveform
Square-wave
Frequency (Hz)

Figure 6:

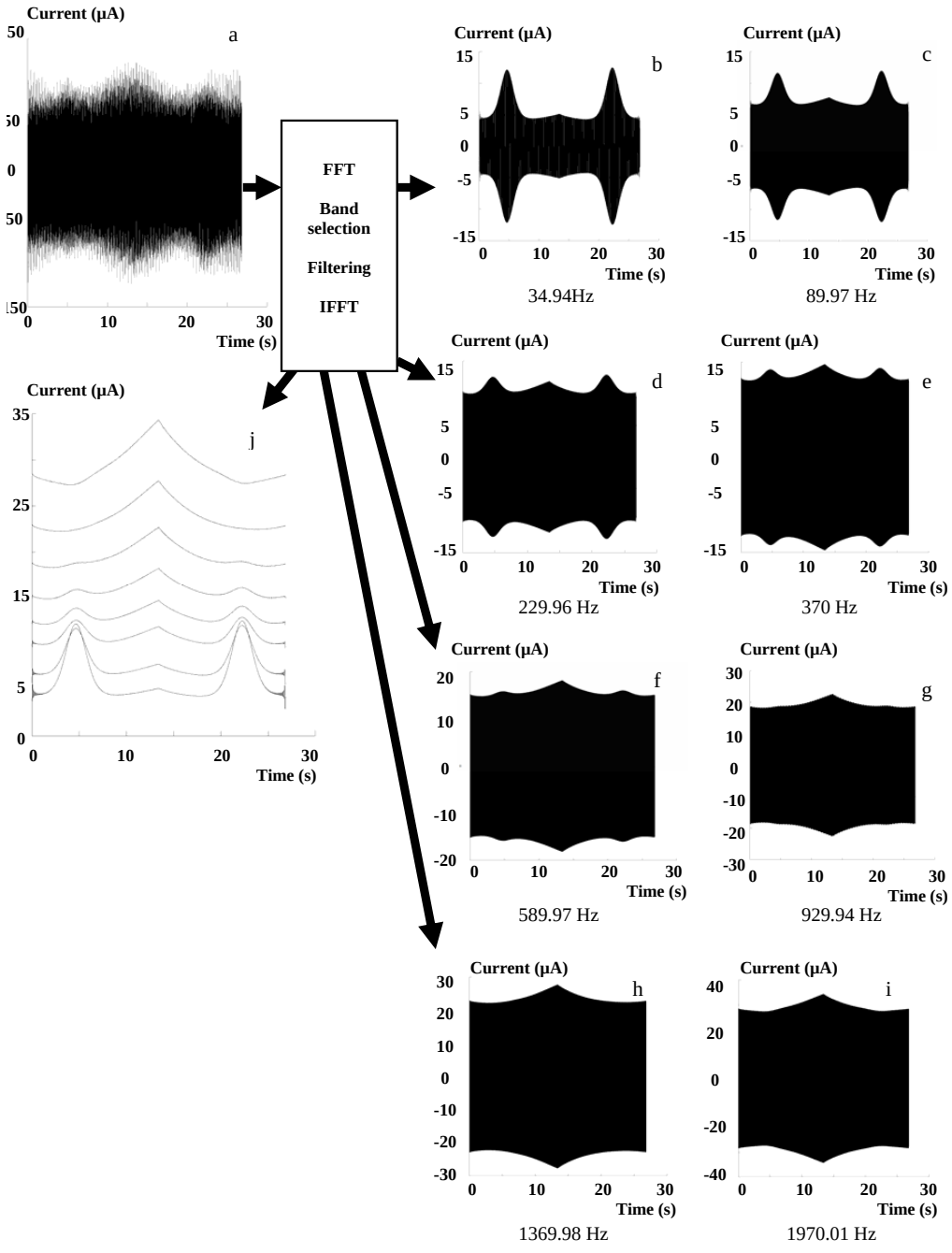
Current (μA)
a
Time (s)
FFT
Band selection
Filtering
IFFT
Current (μA)
b
Time (s)
34.94Hz
Current (μA)
c
Time (s)
89.97 Hz
Current (μA)
d
Time (s)
229.96 Hz
Current (μA)
e
Time (s)
370 Hz
Current (μA)
f
Time (s)
589.97 Hz
Current (μA)
g
Time (s)
929.94 Hz
Current (μA)
h
Time (s)
1369.98 Hz
Current (μA)
i
Time (s)
1970.01 Hz
Current (μA)
j
Time (s)

Figure 7:

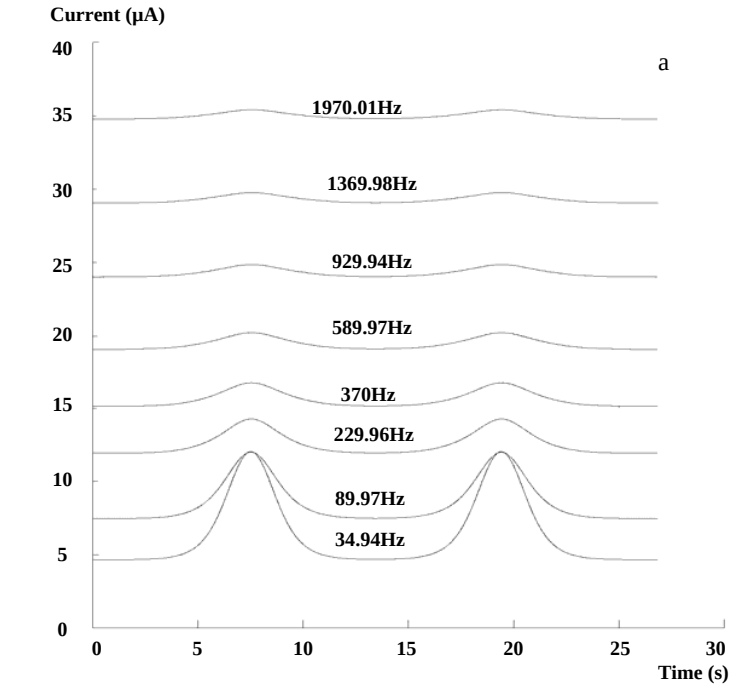
Current (μA)
a
1970.01Hz
1369.98Hz
929.94Hz
589.97Hz
370Hz
229.96Hz
89.97Hz
34.94Hz
0
5
10
15
20
25
30
35
40
Time (s)

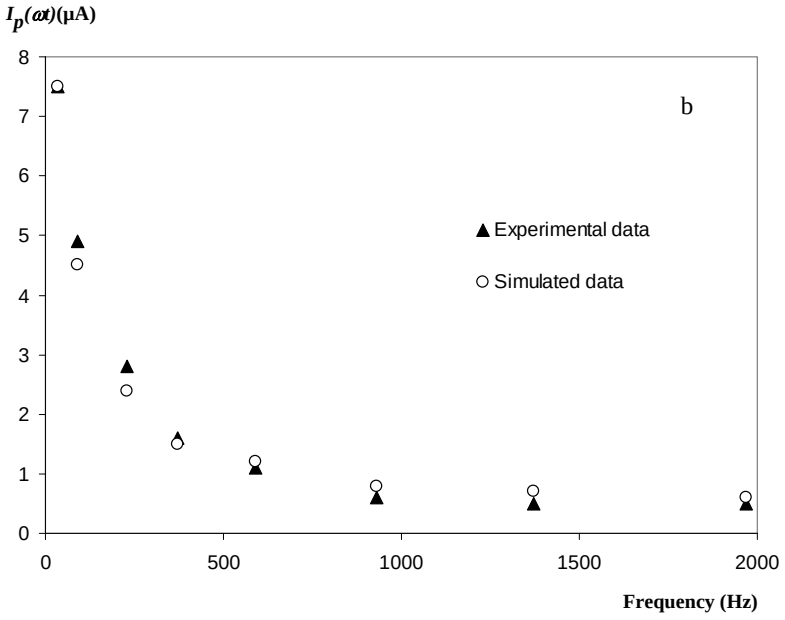
$I_p(\omega t)$(μA)
b
Experimental data
Simulated data
0
1
2
3
4
5
6
7
8
500
1000
1500
2000
Frequency (Hz)

Figure 8:

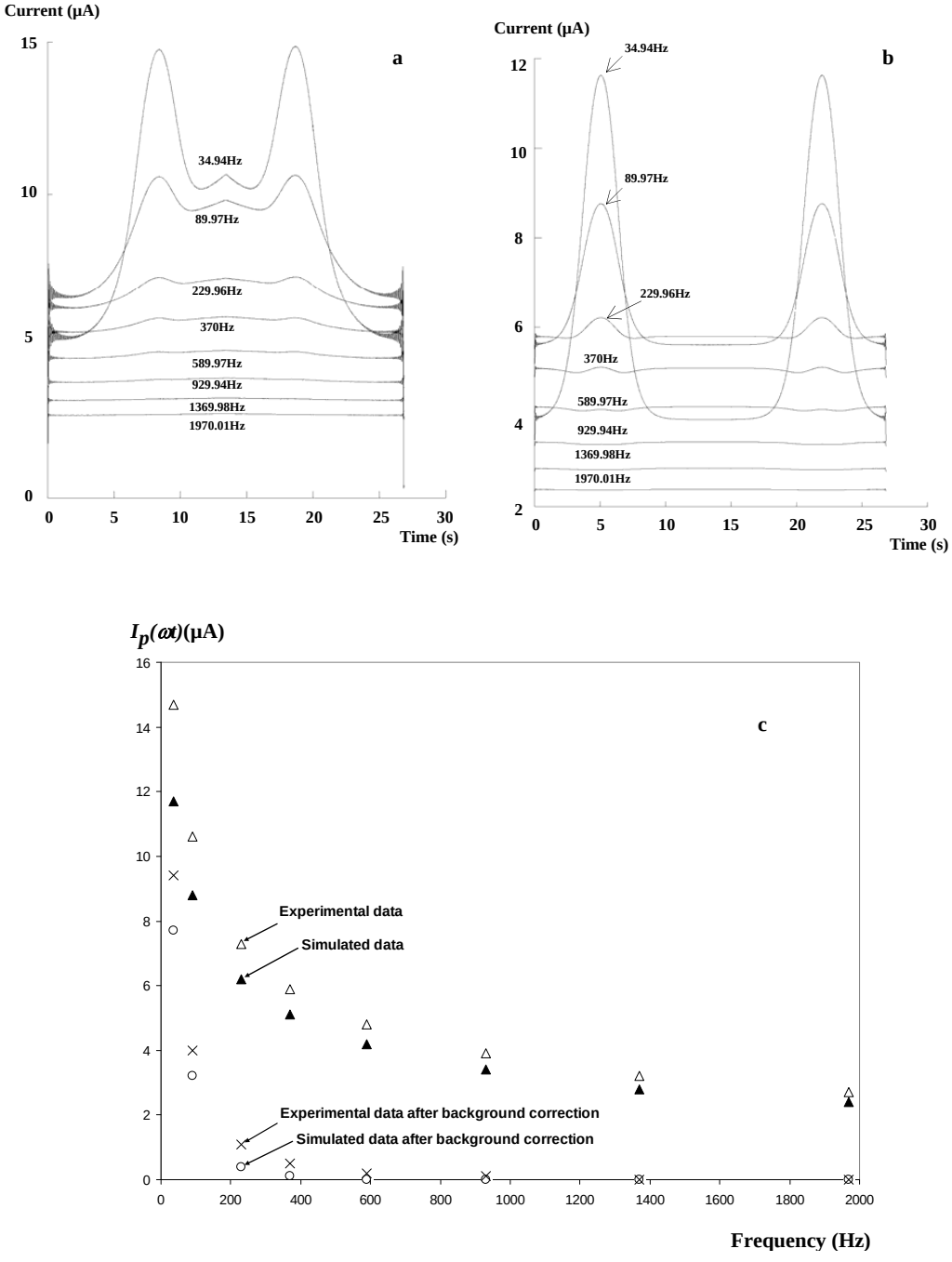
Current (μA)
a
34.94Hz
89.97Hz
229.96Hz
370Hz
589.97Hz
929.94Hz
1369.98Hz
1970.01Hz
Time (s)
Current (μA)
b
34.94Hz
89.97Hz
229.96Hz
370Hz
589.97Hz
929.94Hz
1369.98Hz
1970.01Hz
Time (s)
$I_p(\omega t)$(μA)
c
Experimental data
Simulated data
Experimental data after background correction
Simulated data after background correction
Frequency (Hz)

Figure 9:

Supplementary Material for Designer Based Fourier Transformed Voltammetry: A Multi-frequency, Variable Amplitude, Sinusoidal Waveform

Yongjun Tan[a, 1] Gareth P. Stevenson[b] Ruth E. Baker[c]
Darrell Elton[d] Kathryn Gillow[b] Jie Zhang[e]
Alan M. Bond[a, *] David J. Gavaghan[b, *]

[a]School of Chemistry, Monash University, Clayton, Melbourne, Victoria 3800, Australia.

[b]Oxford University Computing Laboratory, Wolfson Building, Parks Road, Oxford, OX1 3QD, United Kingdom.

[c]Centre for Mathematical Biology, Mathematical Institute, 24-29 St. Giles', Oxford OX1 3LB, United Kingdom.

[d]Department of Electronic Engineering, Latrobe University, Bundoora, Victoria 3083, Australia.

[e]Institute of Bioengineering and Nanotechnology, 31 Biopolis Way, The Nanos, Singapore 138669.

[1]Present address: School of Applied Chemistry, Curtin University of Technology, Perth, Australia.

[*]Corresponding authors. Alan M. Bond, email: Alan.Bond@sci.monash.edu.au, telephone: +61 3 9905 1338, fax: +61 3 9905 4597. David J. Gavaghan, email: David.Gavaghan@comlab.ox.ac.uk, telephone: +44 1865 610667, fax: +44 1865 610670.

Supplementary Figure Legends

Figure S-1. (a) I-t data simulated to mimic experimental data displayed in 2(a). (b) FT-recovered fundamental harmonics simulated to mimic experimental data displayed in Figure 2(b). Parameters used in simulation of a reversible process are provided in the text.

Figure S-2. (a) I-t, (b) fundamental harmonic, data simulated with zero background current in order to mimic experimental data displayed in Figure 2(e) and (f). Parameters used to simulate the reversible process are provided in the text and as for Figure S-1 except $C_{\mathrm{dl}} = 0$ Fm^{-2}.

Figure S-3. Comparison of fundamental harmonic background currents before and after addition of FcMeOH. (a) $I(\omega t)$ versus t data at GC electrode in 0.5 M KCl. (b) as for (a) but after addition of 2.0 mM FcMeOH. (c) Comparison of fundamental harmonic background currents before and after FcMeOH addition.

Figure S-4. (a) Raw current versus time data obtained when 0.100 mM FcMeOH is oxidised at a GC electrode in 0.50 M KCl electrolyte. (b and c) Background corrected current using different designated time regimes: (b) with 0.5-1.5 and 11-12 s, and (c) with 0-1 and 10-11 s correction reference zones.

Supplementary Figures

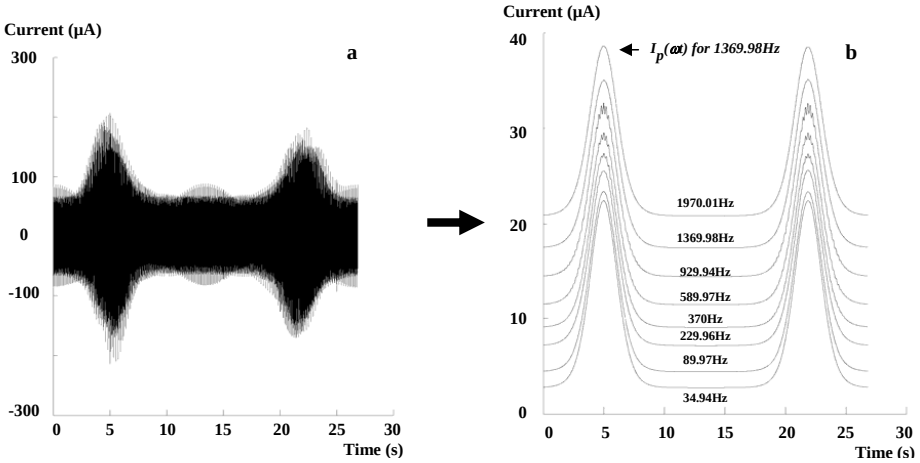

Figure S-1:

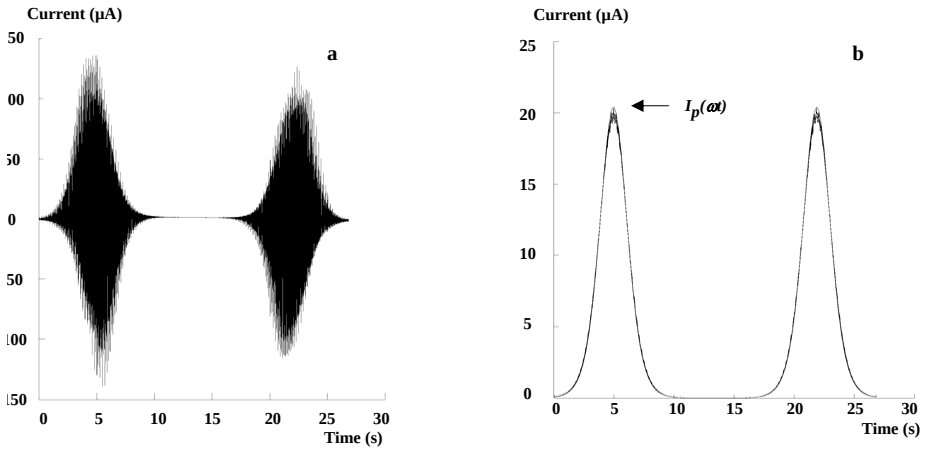

Figure S-2:

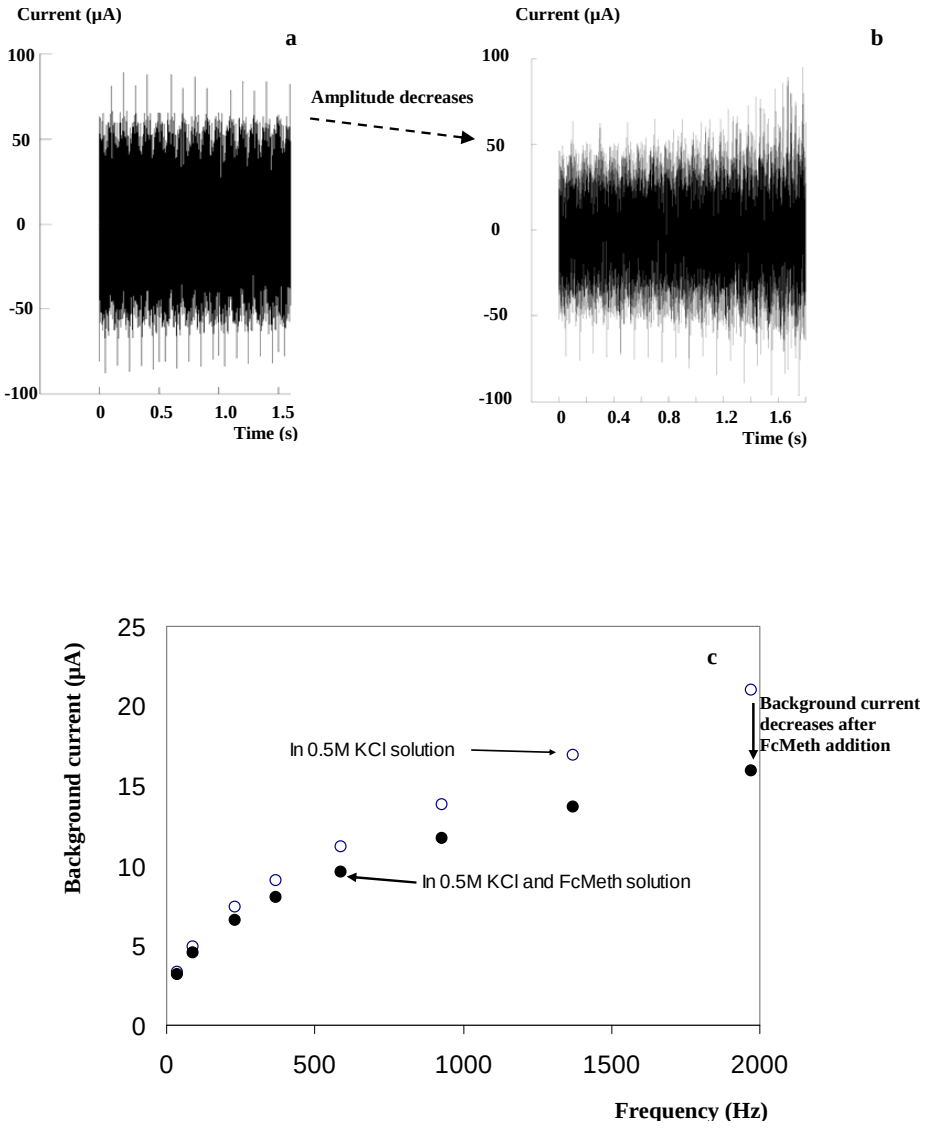
Current (µA)
a
100
50
0
-50
-100
0
0.5
1.0
1.5
Time (s)
Amplitude decreases
Current (µA)
b
100
50
0
-50
-100
0
0.4
0.8
1.2
1.6
Time (s)
c
Background current (µA)
25
20
15
10
5
0
0
500
1000
1500
2000
Frequency (Hz)
In 0.5M KCl solution
In 0.5M KCl and FcMeth solution
Background current decreases after FcMeth addition

Figure S-3:

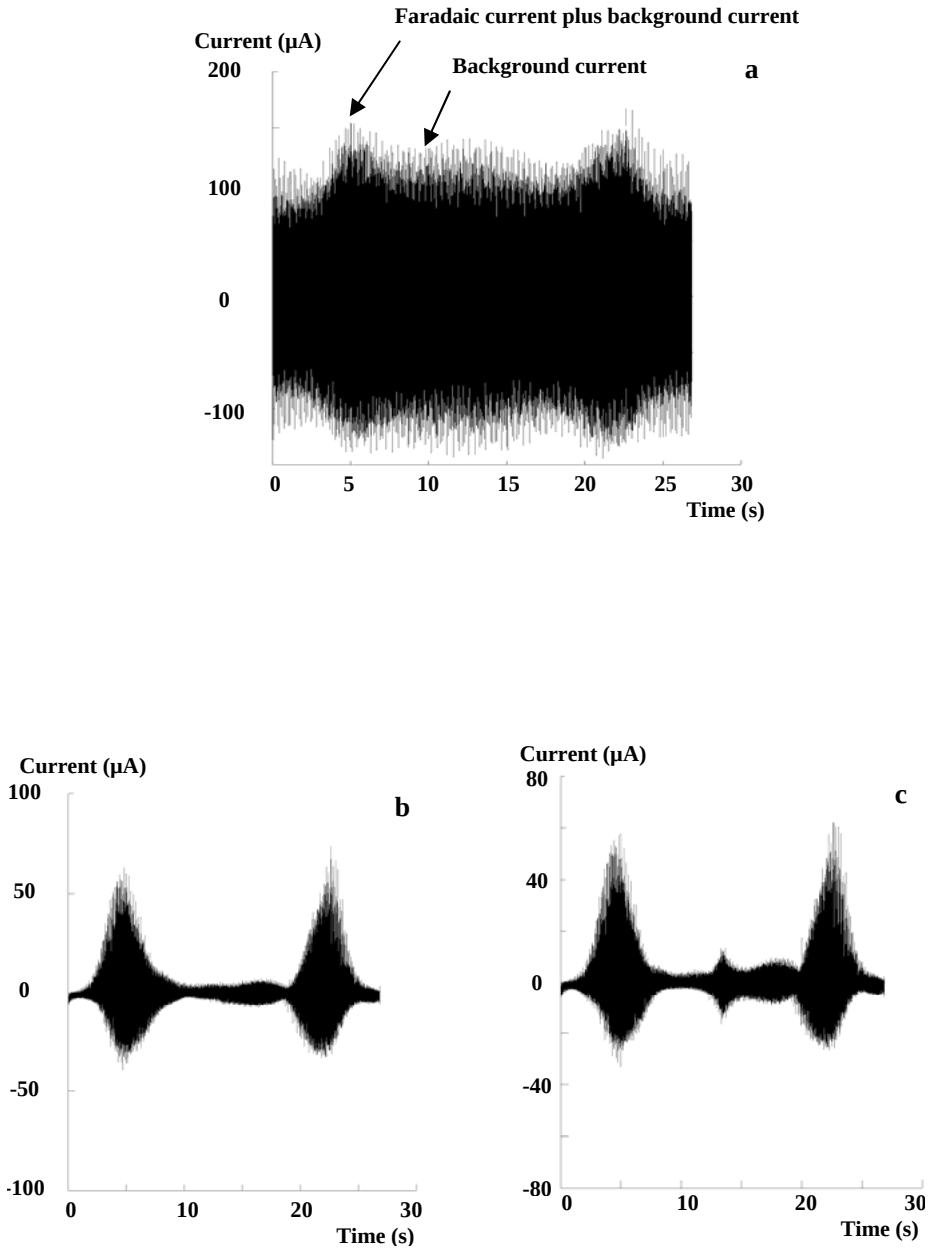
Faradaic current plus background current
Current (µA)
Background current
a
200
100
0
-100
0
5
10
15
20
25
30
Time (s)
Current (µA)
b
100
50
0
-50
-100
0
10
20
30
Time (s)
Current (µA)
c
80
40
0
-40
-80
0
10
20
30
Time (s)

Figure S-4: